THE JOURNAL OF BIOLOGICAL CHEMISTRY VOL. 289, NO. 25, pp. 17812–17829, June 20, 2014

Conserved Modular Domains Team up to Latch-open Active Protein Kinase Cα*

Received for publication, November 13, 2013, and in revised form, March 21, 2014 Published, JBC Papers in Press, April 30, 2014, DOI 10.1074/jbc.M113.534750

Carter J. Swanson[‡1], Michael Ritt[§], William Wang[§¶], Michael J. Lang[§], Arvind Narayan[‖], John J. Tesmer[‡], Margaret Westfall[¶‖], and Sivaraj Sivaramakrishnan[‡§‖2]**

*From the [‡]Biophysics Program, [§]Department of Cell and Developmental Biology, [¶]Department of Cardiac Surgery, [‖]Department of Biomedical Engineering, Life Sciences Institute, and the **Departments of Pharmacology and Biological Sciences, University of Michigan, Ann Arbor, Michigan 48109*

Background: Protein kinase C (PKC) is a nodal regulator of cell signaling.
Results: Multiple interactions between conserved regulatory domains in PKC synergistically stabilize a nanomolar affinity homodimer critical for cellular function.
Conclusion: Homodimerization regulates the equilibrium between the auto-inhibited and active states of PKCα.
Significance: Multiplexed interactions between modular domains dictate PKC function.

Signaling proteins comprised of modular domains have evolved along with multicellularity as a method to facilitate increasing intracellular bandwidth. The effects of intramolecular interactions between modular domains within the context of native proteins have been largely unexplored. Here we examine intra- and intermolecular interactions in the multidomain signaling protein, protein kinase Cα (PKCα). We identify three interactions between two activated PKC molecules that synergistically stabilize a nanomolar affinity homodimer. Disruption of the homodimer results in a loss of PKC-mediated ERK1/2 phosphorylation, whereas disruption of the auto-inhibited state promotes the homodimer and prolongs PKC membrane localization. These observations support a novel regulatory mechanism wherein homodimerization dictates the equilibrium between the auto-inhibited and active states of PKC by sequestering auto-inhibitory interactions. Our findings underscore the physiological importance of context-dependent modular domain interactions in cell signaling.

The use of modular protein domains has emerged as a prominent feature of increasing phylogenetic complexity (1, 2). Linking modular domains within a single protein allows complex regulation while conserving the sequence and structure of the individual domains, especially for those that have catalytic activity (3). For instance, spatiotemporal control of signaling proteins is often achieved by stringing together a conserved catalytic domain with one or more regulatory modules. These modules can play multiple roles including masking the catalytic site to inhibit basal activity (auto-inhibition), releasing auto-inhibition through conformational changes triggered by second messenger stimuli, and facilitating translocation to subcellular compartments through binding secondary messengers or scaffolding proteins. Each additional module in a signaling protein provides a combinatorial enhancement to its regulation and cellular function (4). The protein-context independent structure and cellular function of individual modules have been extensively researched using biophysical approaches such as x-ray crystallography and NMR spectroscopy (5). However, coordination of interactions between domains in intact proteins remains unexplored primarily due to the reliance on reductionist structural and biochemical approaches. As a corollary, our current structural understanding of modular signaling proteins does not adequately address the versatility of their cellular function (6–8). In this study we overcome this limitation with a technique we previously developed to systematically modulate interactions between individual protein domains in the context of the entire molecule (9, 10).

Generally, stark perturbations are required to study intramolecular interactions in proteins. For instance, to measure the strength of an intramolecular interaction between two domains it is typical to split them into two individual peptides (11). An alternative approach is to truncate or mutagenize a proposed interaction interface and look at a functional consequence associated with the loss of the interaction (12–14). In the first approach the strength of an interaction can be underestimated given that when the two interacting domains are in the same polypeptide, they will likely have a high local concentration that can affect the on-rate of the interaction. In the second approach, it is often difficult to anticipate whether a change in function is directly or tangentially effected by the truncation or mutagenesis.

To address the technical shortcoming in studying intramolecular domain-domain interactions, we previously developed and applied a novel genetic method termed Systematic Protein Affinity Strength Modulation (SPASM) (10). This technique utilizes an ER/K motif that has unusual biophysical properties (15). The ER/K motif primarily adopts an extended α-helical secondary structure in solution with an end-to-end distance of 10–30 nm, depending on the length of the motif (16). However, it is prone to stochastic breaks in helicity that allow the N and C termini of the helix to come in close proximity of each other at a low but predictable frequency (10). Capitalizing on this phe-

* This work was supported, in whole or in part, by National Institutes of Health Grant 1DP2 CA186752-01 (to S. S.). This work was also supported by American Heart Association Scientist Development Grant 13SDG14270009 (to S. S.).
[1] Supported in part by the MCubed program at the University of Michigan.
[2] To whom correspondence should be addressed: Dept. of Cell and Development Biology, 3045 BSRB, 109 Zina Pitcher Place, Ann Arbor, MI 48109-2200. Tel.: 734-764-2493; Fax: 734-763-1166; E-mail: sivaraj@umich.edu.

nomenon, a genetically encoded FRET pair as well as interacting polypeptides can be fused to either end of the ER/K motif to build a single polypeptide (*x*polypeptide-FRETdonor-ER/K linker-FRETacceptor-*y*polypeptide) (9, 17). At low (nM) concentrations, the interaction between the polypeptides will report a binary high FRET interacting state or low FRET non-interacting state that will be averaged out in ensemble measurements (10). It has been empirically determined that the on-rate for interactions in this system are dictated by the frequency that the α-helix stochastically brings its ends in close proximity, whereas the off-rate is dependent on the interaction between the polypeptides attached to the end of the helix (10). Additionally, the frequency at which the ends of the α-helix come in close proximity is a function of the length of the α-helix; longer helices have a lower frequency of end-to-end proximity (10). By incorporating different length ER/K motifs between interacting polypeptides, the on-rate can be modulated such that the apparent concentrations can be varied from 100 nM to 10 μM (10). Finally, the SPASM module is a transposable genetic element that can be incorporated into naturally occurring linkers between modular domains in most proteins. This technology allows intramolecular interactions to be perturbed in systematic ways such that domain-domain interactions can be directly observed and characterized (9). Here we utilize this technology to explore domain-domain interactions in the multidomain protein kinase C (PKC).

The PKC family exemplifies the use of modular architecture in cellular function. PKC is composed of a conserved catalytic domain (CD)[3] fused to multiple, modular regulatory domains (RDs: pseudo-substrate, C1a, C1b, and C2) that are sensitive to different small molecule/second messenger stimuli (α isoform: C1a-diacylglycerol (DAG) and phorbol ester (PMA); C1b-DAG, PMA; C2- Ca^{2+}). In the absence of stimuli, the RDs cooperatively mask the catalytic site, whereas conformational changes facilitated by effector binding to these domains facilitate interactions with cellular membranes and scaffolding proteins (6). Although numerous studies have dissected the structure-function relationship of the individual regulatory modules, interactions between modules remain largely unexplored. Hence, the current model of PKC activation presents it as a binary switch that is basally turned off through a RD-CD interaction and is switched on when effectors bind and release the RD from the CD (18, 19). As a glimpse beyond this binary view, a high affinity intermolecular interaction between the effector-bound C1 and RD (12 nM) has been previously reported (11). Furthermore, PKC activation has been proposed to trigger homodimerization (20) with a consequent influence on catalytic activity (11, 20). However, these intermolecular interactions have not been incorporated into current models of PKC activation, presumably due to the lack of mechanistic or structural details.

[3] The abbreviations used are: CD, catalytic domain; RD, regulatory domain; DAG, diacylglycerol (1,3-diolein); PMA, phorbol-12-myristate-13-acetate; BimI, bisindoylmaleimide I; PS, 1,2-diacyl-*sn*-glycerol-3-phospho-L-serine; BMH, bismaleimidohexane; MBP, myelin-binding protein; LPA, lysophosphatidic acid; mCit, mCitrine; mCer, mCerulean; ROCK, Rho-associated kinase I and II; TEV, tobacco etch virus; TM, turn motif; SPASM, Systematic Protein Affinity Strength Modulation.

Here, we demonstrate that PKCα readily homodimerizes upon stimulation with activating effectors *in vitro*. We generated and characterized a unimolecular FRET sensor that is both functional as PKCα and reports on effector-induced dimerization *in vitro* and in CHO cells. We then used multiple FRET sensors, some including the ER/K linker, to dissect domain-domain interactions in the activated state of PKCα to reveal that dimerization stems from several weak interactions involving the C1, C2, and catalytic domains that together contribute to a nanomolar affinity interaction. We then address the functional significance of PKCα dimerization through four separate vignettes. 1) We found that the *in vitro* specific activity of PKCα is more sensitive to dimerization than it is to modulation of the auto-inhibitory interactions. 2) We observed homodimerization in the basal state upon mutagenesis of the turn motif priming phosphorylation site (Thr → Ala), a finding with implications in PKC maturation. 3) We revealed that PKC function in cells can be modulated in the presence of peptides designed to destabilize the dimer state. 4) We observed that a commonly used PKC inhibitor bisindoylmaleimide I (BimI) can alter PKCα localization by destabilizing basal, auto-inhibitory interactions. We conclude with a simple model in which dimerization allows PKC to overcome a high degree of basal auto-inhibition by latching open the effector stimulated kinase.

EXPERIMENTAL PROCEDURES

Reagents—1,3-Diolein (DAG) (Sigma) and 1,2-diacyl-*sn*-glycerol-3-phospho-L-serine (PS) (Sigma) were solubilized in chloroform. Aliquots of DAG and PS were dried and resuspended into a 20 mM HEPES, 5 mM $MgCl_2$, and 0.1 mM EGTA buffer (500 and 250 μg/ml, respectively) and used as a 10× stock for standard LC conditions (refreshed biweekly) (sonicated prior to each experiment). Phorbol-12-myristate-13-acetate (PMA) was purchased from Calbiochem and solubilized in DMSO. Bismaleimidohexane (BMH) was purchased from Pierce and solubilized in DMSO immediately before cross-linking experiment. BimI was purchased from Calbiochem. *N*-Methylanthraniloyl (MANT)-ADP was purchased from Invitrogen. The myristoylated RD peptide corresponding to residues 218–226 (Myr SLNPEWNET) was purchased from Sigma (P0102), and the scrambled RD peptide (Myr NPESNLTWE) as well as the CD peptide corresponding to residues 633–642 (Myr GQPVLTPPDQ) and scrambled CD peptides (Myr QPGQPDLPVE) were custom-synthesized by GenScript. All peptides were solubilized in slightly basic water (~pH 8.5). Priming phosphorylations were assessed using Ser(P)-657 (06-822 Millipore) and Thr(P)-638 (32502 ABCAM) antibodies according to manufacturer's protocol.

Constructs—All PKC constructs were cloned from full-length human cDNA (Open Biosystems) using PCR into unique restriction sites in pBiex1 (Novagen) or pcDNA/FRT (Invitrogen) plasmid vectors. All constructs contain a C-terminal FLAG tag. $(Gly\text{-}Ser\text{-}Gly)_{2-4}$ linkers separate fluorophores from PKC domains. In the SPASM constructs, linkers separate fluorophores from the ER/K α-helix and the PKC domains. The Tev protease site was engineered at the N terminus of the ER/K α-helix. Details on the ER/K α-helices have been previously reported (10). Domain truncation constructs were created by

site-directed mutagenesis using Pfu-Turbo (Agilent). In Fig. 6, *a* and *f*, the following truncations were made: 32–151 (ΔC1), 158–292 (ΔC2), 606–672 (ΔC-tail), 32–100 (Δ C1a), or 101–151 (Δ C1b). In Fig. 6 we define the CD (catalytic domain, 336–672) and RD (regulatory domains, 1–335). Constructs were analyzed for kinase activity and Ser-657 and Thr-638 phosphorylation (see Fig. 2) or in the absence of kinase activity MANT-ADP binding (see Fig. 2, *f–h*).

Insect Cell Culture and Protein Purification—Sf9 cultures in Sf900-II media (Invitrogen) were transiently transfected with pBiex1 vectors using Escort IV transfection reagent (Sigma). 72 h post transfection, cultures were lysed with 0.5% IGEPAL, 4 mM $MgCl_2$, 200 mM NaCl, 7% Sucrose, 20 mM HEPES, 5 mM DTT, 50 μg/ml PMSF, 5 μg/ml aprotinin, 5 μg/ml leupeptin, pH 7.5. Clarified lysates were incubated with anti-FLAG M2 Affinity resin (Sigma) for 2 h. The resin-bound protein was washed with 20 mM HEPES, 2 mM $MgCl_2$, 300 mM KCl, 2 mM DTT, 50 μg/ml PMSF, 5 μg/ml aprotinin, 5 μg/ml leupeptin, pH 7.5, 3 times with 10× resin volume. The protein was eluted with 100 μg/ml FLAG peptide. The buffer was exchanged to 5 mM HEPES, 0.5 mM EGTA, 1 mM DTT, 5 μg/ml aprotinin, 5 μg/ml leupeptin, and 2 mM $MgCl_2$ at pH 7.5 using Zeba Spin Desalting Columns (Pierce). Protein concentration was determined from fluorescence emission of mCitrine or mCerulean compared with a matched standard (FluoroMax-4, Horiba Scientific) or A280 using extinction coefficients determined by ExPASy Protparam (Swiss Institute of Bioinformatics).

Mammalian Cell Culture—CHO Flp-in cells (Invitrogen) were cultured and incubated in DMEM supplemented with 10% FBS, 4.5 g/liter D-glucose, 1% glutamax, 20 mM HEPES, pH 7.5, and 1% antibiotic-antimycotic (Invitrogen) at 37 °C and 5% CO_2. Constructs in the pcDNA vector were transiently transfected into CHO cells using FuGENE HD (Promega) and harvested after 48 h. CHO Flp-in cells stably expressing mCerulean (mCer)-PKCα-mCitrine (mCit)-FLAG constructs were generated according to the manufacturer's protocol with cells maintained in 600 μg/ml hygromycin. For live cell imaging, cells were trypsinized, and 2×10^5 cells were re-plated onto 35-mm glass-bottom dishes (MatTek Corp.) coated with 1 μg of fibronectin (Sigma) and allowed to adhere for 2 h. The plates were washed with 2 ml of HEPES-buffered saline with 0.2% dextrose, and 500 μl of this medium was added to the cells before imaging. Cells were imaged at 40× or 60× with a Nikon TiE microscope equipped with an Evolve 512 × 512 EM-CCD camera (Photometrics), a mercury arc lamp, and the appropriate band pass filters. For FRET images, a Dual-View filter (Photometrics) was used for simultaneous acquisition of mCerulean and mCitrine peak fluorescence. After image acquisition of untreated condition (pre), cells were perfused with HBS containing 10 μM PMA and 900 μM $CaCl_2$ or 50 μM LPA at room temperature. For live cell fluorometer experiments (Figs. 2*a* and 8c), 1 confluent 10-cm plate was trypsinized, washed with 10 ml of DMEM with 10% FBS to inactivate the trypsin, and washed twice with 5 ml of HBS with 0.2% dextrose before being resuspended in 1 ml. This is similar to methods previously reported (17). All conditions involving myristoylated peptides were incubated with 20 μM peptide for 15 min before imaging or fluorometer experiments. For translocation imaging experiments 1.5 μM BimI was added to cells 2–4 min before image acquisition.

Fluorometer Data Acquisition—A Fluoromax-4 fluorometer (Horiba Scientific) was used to obtain FRET spectra. Samples were excited at 430 nm (8-nm band pass), and the emission was recorded from 450 to 650 nm in 1-nm intervals (4-nm band-pass). For unimolecular sensors, 20–80 nM protein was used *in vitro*, and for bi-molecular sensors, 40 nM mCerulean and 160 nM mCitrine constructs were used unless otherwise noted. All *in vitro* assays were performed in a buffer containing 20 mM HEPES, 5 mM $MgCl_2$, 500 μM EGTA, 1 mM DTT, 5 μg/ml aprotinin, and 5 μg/ml leupeptin and were mixed in tubes precoated with 0.1 mg/ml BSA. Final concentrations of 1.5 mM $CaCl_2$, 3.2 μM PMA, 10 μM BimI, or 50 μg/ml DAG and 25 μg/ml PS were added to the sample where indicated. All conditions were allowed to equilibrate for >30 min at 30 °C after the reaction was fully mixed. The figures of FRET depict mean and S.E. from three independent spectra obtained using the same batch of recombinant protein and the same reagent preparations on the same day and are representative of results observed from three independent measurements. For experiments monitoring MANT-ADP, binding samples were prepared in the same manner but obtained spectra with direct excitation of tryptophan at 290 nm (8-nm band pass), and emission was recorded from 300 to 550 nm at 1-nm intervals (4-nm band pass) or direct excitation of MANT at 340 nm (4-nm band pass) from 400 to 550 nm at 1-nm intervals (2-nm band pass).

Bimolecular RD-RD, RD-CD, and CD-CD FRET Assay—The appropriate combination of TEV protease-treated RD-mCer-TEV-30-nm ER/K-CD-FLAG, RD-mCit-TEV-30 nm ER/K-CD-FLAG, RD-TEV-30 nm ER/K-mCer-CD-FLAG, and RD-TEV-30 nm ER/K-mCit-CD-FLAG constructs were used to probe the individual bimolecular RD-RD, RD-CD, and CD-CD interactions. Coomassie-stained or fluorescent protein-scanned SDS-PAGE was used to verify complete TEV cleavage (data not shown).

Kinase Assay—Kinase assays were performed using the Kinase-Glo Max Luminescence assay kit (Promega) according to the manufacturer's protocol. Synthetic liposomes were made from Brain Polar Lipid Extract (Porcine) (Avanti; high in PS) mixed with 2% w/w 1,3-diolein (Sigma) using established procedures (21). Briefly, the liposomes were suspended in chloroform for storage and dried under nitrogen and stored under vacuum for 18 h. The mixture was resuspended to a concentration of 12.5 mg/ml in HEPES buffer and underwent at least three freeze-thaw cycles in liquid nitrogen then hot water. The mixture was then extruded (Avanti) using a 0.08-μm Nuclepore Track-Etch Membrane (Whatman) and diluted into a 20× reaction concentration of 1.6 mg/ml. Histone IIIs (Sigma), bovine myelin-binding protein (MBP; Sigma), or MBP residues 4–14 (Santa Cruz Biotechnology, Inc) at final concentrations of 40 μM were used as substrates unless otherwise noted. The reaction was initiated with 40 μM ATP (Sigma) and were briefly mixed and incubated with mild shaking at 30 °C from 2 to 10 min. For all conditions the ATP consumption is calculated against a matched control without kinase. ATP calibration curves were obtained under identical conditions (without

kinase). End-point luminescence was measured in white, 96-well plates (Thermo Scientific) on a Synergy HT (Biotek).

Cross-linking Assay—A cross-linking assay was performed as previously reported (20). Briefly, 200–400 nM PKC was preincubated in a HEPES buffer containing 2% glycerol and 0.02% Triton X-100 and the indicated effectors. A 50× stock of BMH (1.25 mM) in DMSO was added to the preincubated solution for 2–5 min then quenched with 5× SDS-PAGE loading dye with 20 mM DTT. All blots shown are representative of at least three independent experiments. It should be noted that the level of cross-linking observed is highly dependent on the concentration of BMH resulting in variability between experiments. To circumvent this limitation inherent in cross-linking assays, the extent of cross-linking is always evaluated with respect to a matched control in each experiment.

In Vitro Membrane Partitioning Assay—This assay was performed as previously described (21). Liposomes were prepared as in the kinase assay except the liposomes were extruded with an equal volume of 340 mM sucrose buffer. Purified protein was clarified at 80,000 rpm, and the clarified protein was incubated in the indicated conditions. The reaction mixture was spun at 80,000 rpm, the supernatant was taken off (soluble fraction), and the remaining pellet was suspended in an equal volume of 1× SDS-PAGE loading dye (pellet fraction).

Western Blotting—Lysates were prepared from stably expressing CHO cells generated using the Flip-in system (Invitrogen). Cells were plated in 6-well dishes (NEST) to reach 80–90% confluence within 24 h and were subsequently serum-starved for an additional 24 h. Cells were treated with the indicated peptides (20 μM) 15 min before the addition of 1-oleoyl lysophosphatidic acid (LPA, Cayman Chemicals, 10 μM). Cells were incubated with LPA for 15 min before lysis on ice with ice-cold buffer (1% Triton X-100, 250 mM NaCl, 50 mM Tris pH 6.8, 4 mM $MgCl_2$, 2 mM EDTA, 1:100 phosphatase inhibitor mixture II (Sigma), and containing 10 μg/ml aprotinin, 10 μg/ml leupeptin, and 1 mM PMSF). Lysates were syringed with a 26-gauge needle and clarified by spinning at 16,000 × *g* (10 min, 4 °C). Total lysate protein was assayed either by Bradford assay or by total ERK1/2 blotting (see below) with no significant difference observed between the two methods. Lysates were separated on 10% polyacrylamide, SDS gels before being transferred to PVDF membranes for 3 h at 300 mA. Blots were blocked with 2% BSA, TBS + 0.1% Tween (TBST) for 1 h at room temperature. Primary phospho ERK1/2 antibody (4376S, Cell Signaling) was used at a concentration of 1:5000 in 2% BSA/TBST and incubated overnight at 4 °C. Blots were washed with TBST (3 × 10 min) before the addition of secondary antibody (goat anti-rabbit (Jackson ImmunoResearch Laboratories, Inc.) 1:10,000 in 1% milk/TBST). Blots were washed again with TBST (3 × 10 min) and developed using Immobilon Western chemiluminescent HRP substrate (Millipore). Blots were imaged using a ChemiDoc-it imaging system (UVP). Blots were stripped with Restore PLUS Western stripping buffer (Thermo Scientific) and reblotted with total ERK1/2 antibody (4695S, Cell Signaling; 1:10,000, 2% BSA/TBST). Blots were exposed to secondary as above and developed under the same conditions. All blots shown are representative of at least three independent experiments. Cross-linked PKC was probed (Fig. 1*f*) using a PKCα antibody (sc-8393, Santa Cruz Biotechnology, 1:10,000 in 2% BSA/TBST).

Live Cell FRET Analysis—Images were analyzed using custom software in Matlab (Mathworks Inc.). Briefly, for images of LPA-induced cells with constant excitation over the second-to-min time scales, images were subjected to a background threshold/subtraction followed by correction for photobleaching using a maximum threshold. FRET ratios were computed as the pixel-by-pixel ratio between mCitrine and mCerulean intensities across the time series. For images of PMA-induced cells in which excitation and image acquisition occurred for 200–500 ms every 30 s for 15–20 min, the straight pixel-by-pixel ratio was calculated, as little photobleaching effects were observed. Deconvolution was performed using AutoQuant X3 (MediaCybernetics).

Dissociation Constant of Dimer Formation—The equilibrium between mCer-PKCα-mCit (*F*, fluorescent) and PKCα-FLAG (*D*, dark) can be represented by the following five equations, where F_t and D_t are the total concentrations of mCer-PKCα-mCit and PKCα-FLAG, respectively.

$$F + F \leftrightarrow F \cdot F \quad \text{(Eq. 1)}$$

$$+$$

$$D + D \leftrightarrow D \cdot D \quad \text{(Eq. 2)}$$

$$\updownarrow$$

$$D \cdot F \quad \text{(Eq. 3)}$$

$$F_t = F + F \cdot F + D \cdot F \quad \text{(Eq. 4)}$$

$$D_t = D + D \cdot D + D \cdot F \quad \text{(Eq. 5)}$$

Assuming the three interactions are equivalent and interchangeable, knowledge of the dissociation constant (K_D) is necessary and sufficient to explicitly calculate the partitioning between the species. A custom Matlab substitution solver was used to numerically calculate each of the five species (*F, D, F·F, D·F, D·D*) for a range of K_D values. Knowledge of the individual species allows us to estimate the K_D by evaluating the best fit (least squares) to the titration curve of measured FRET ratio (R_{obs}) as a function of PKCα-FLAG concentration (D_t). As previously reported, R_{obs} can be expressed as a linear combination of the FRET ratio for the dimer ($R_{F\cdot F}$), monomer (R_F), and interspecies dimer ($R_{D\cdot F}$),

$$R_{obs} = R_{F\cdot F}(F \cdot F/F_t) + R_F(F/F_t) + R_{D\cdot F}(D \cdot F/D_t) \quad \text{(Eq. 6)}$$

$R_{F\cdot F}$ is set to the observed FRET ratio at saturating concentrations (>100 nM) of mCer-PKCα-mCit, $R_{D\cdot F}$ is set to the observed FRET ratio at high D_t/F_t ratios (>20), and R_F is set to the basal FRET level in the absence of effectors. With these constraints and K_D as the only free parameter, we find that a $K_D < 5$ nM provides an indistinguishable fit to the experimental measurements. This competitive binding measurement with interchangeable, equivalent species can only provide an upper bound to the K_D rather than a precise measurement. Lower concentrations of the mCer-PKCα-mCit can be used to improve this estimate; however, they suffer from low signal-to-noise in our fluorometer measurements.

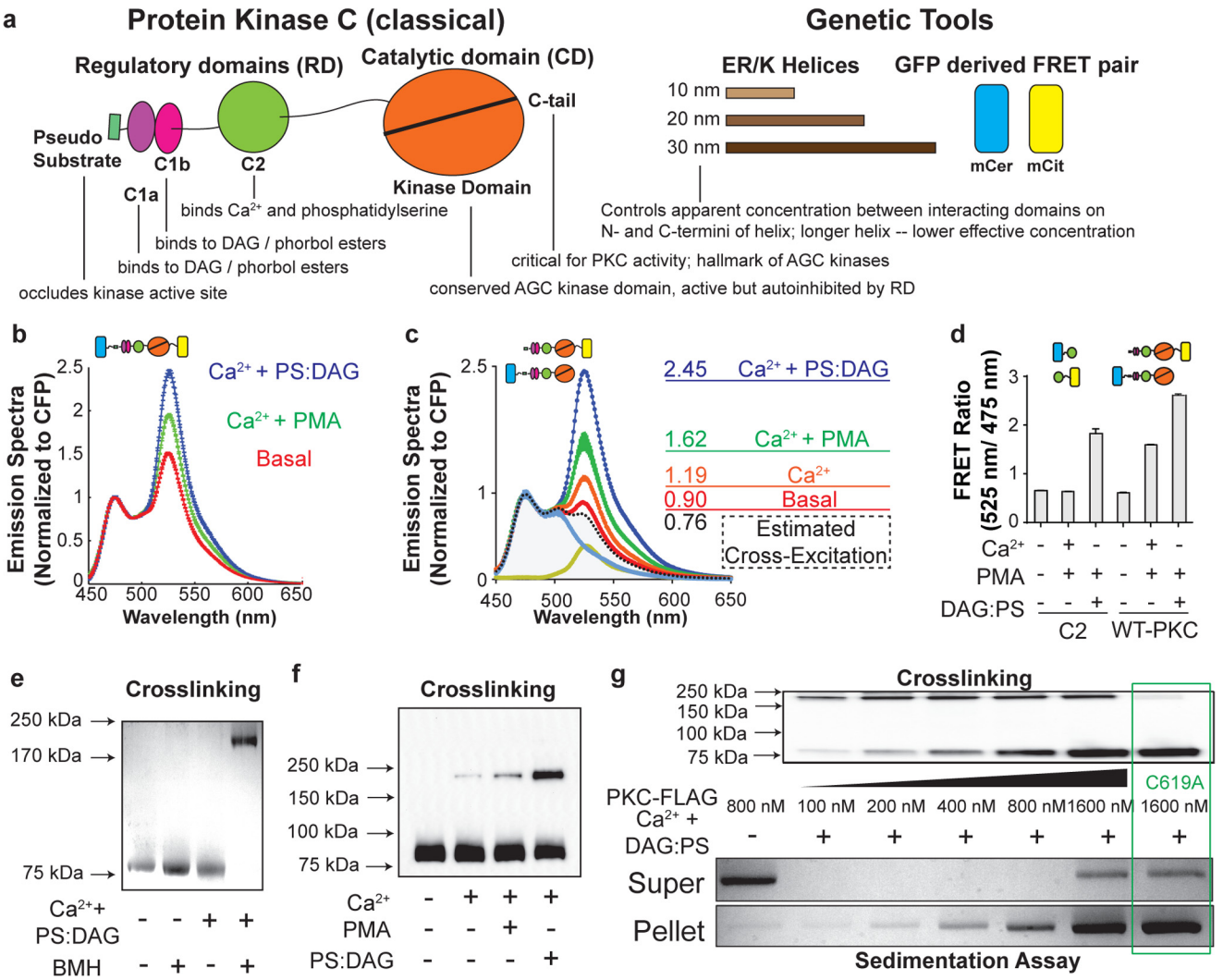

FIGURE 1. **Homodimerization of activated recombinant PKCα.** *a*, schematic of PKCα and the genetic tools used in the study. Subsequent figures utilize this scheme to depict FRET reporters (written/depicted *left-to-write* or *top-to-bottom* as N- to-C-terminal). Fluorescent proteins used in this study were mCerulean (*mCer*) and mCitrine (*mCit*). *b* and *c*, FRET increases after treatment of sensors with different effector combinations. FRET spectra normalized to the FRET donor (mCer) after effector stimulation of recombinant sensor protein. Shown are emission spectra of mCer-PKCα-mCit (50 nM) (*b*) or mCer-PKCα (30 nM) (*c*) and PKCα-mCit (100 nM) excited at 430 nm in the presence of EGTA (*Basal*) or with 1.5 mM $CaCl_2$ or the combination of effectors 1.5 mM $CaCl_2$ and 3.2 μM PMA or 750 μM $CaCl_2$ and 50 μg/ml DAG and 25 μg/ml PS. In *c* the emission of 30 nM mCer-PKCα (*light blue*) and 100 nM PKCα-mCit (*yellow*) was obtained separately after donor excitation at 430 nm in the presence of EGTA, and the two spectra were added and normalized to the peak donor (mCer) emission value at 475 nm to estimate the FRET-independent cross-excitation of the acceptor mCit. *CFP,* cyan fluorescent protein. *d*, bimolecular FRET sensors composed of the C2 domain (residues 185–292) or full-length PKC, fused to mCit or mCer, at matched concentrations under the specified conditions. The C2 domain shows an increase in FRET after activation with Ca^{2+} + PS/DAG but not Ca^{2+} + PMA. Both activation conditions result in an increase in FRET greater in the full-length sensors relative to the C2 domain sensors. *Error bars*, S.E. $n \geq 3$. *e* and *f*, cross-linking of recombinant protein shows homodimer formation after effector stimulation. *e*, representative SDS-PAGE of disulfide cross-linked PKCα-FLAG. BMH (2-min incubation) increases the apparent molecular weight of PKCα by ~2.5 fold in the presence of 750 μM $CaCl_2$ and 50 μg/ml DAG and 25 μg/ml PS. *f*, a representative immunoblot using an anti-PKCα antibody resolves single BMH cross-linked bands of equivalent mass but differing intensities after incubation of PKCα-FLAG with indicated effectors as in *c*. *g*, increasing concentrations of PKCα result in a constant amount of cross-linked protein despite increased PKC binding to a fixed density of liposomes. *Top*, representative SDS-PAGE of cross-linked PKCα for a fixed concentration of liposome (~80 μg/ml PS rich brain polar lipid extract (Porcine) mixed with 2% w/w DAG) as a function of increasing concentrations of PKCα-FLAG. All samples were treated with 25 μM BMH for 3 min. The final well includes C619A mutant PKCα-FLAG under matched conditions. *Bottom*, PKCα-FLAG was incubated with or without the sucrose loaded liposomes used in the cross-linking assay (*top*) and fractionated by ultracentrifugation; the supernatant or pellet was subsequently separated by SDS-PAGE. Saturation of the liposomes with PKCα-FLAG occurred at a concentration between 800 and 1600 nM. PKCα-FLAG (C619A) does not cross-link under the same conditions as WT but demonstrates a comparable ability to associate with liposomes.

RESULTS

To investigate the role of intramolecular interactions in the regulation of PKCα, several distinct FRET reporters were used throughout the study. These are composed of discrete domains of PKCα fused to ER/K linkers, and the GFP-derived mCit and mCer FRET pair (Fig. 1*a*) tethered with $(Gly\text{-}Ser\text{-}Gly)_{2-4}$ linkers to allow for rotational freedom. Basally within a cell or in the presence of EGTA *in vitro*, the RDs (includes N- to-C-terminal pseudosubstrate, C1a, C1b, and C2 domains) of PKC are known to engage in *cis* inhibitory intramolecular interactions with the CD (includes the kinase domain and the C-terminal extension termed the C-tail) (18, 22). Furthermore, the small molecules Ca^{2+}, DAG/PMA, and BimI have been established to interact primarily with the C2, C1, and catalytic domains, respectively (6).

PKCα Homodimerizes upon Stimulation with Effectors in Vitro—We engineered an initial unimolecular FRET sensor (mCer-PKCα-mCit-FLAG; each element is listed from the N to the C termini and dashes consist of a $(GSG)_{2-4}$ linker) capitalizing on the design scheme of a previously reported PKCδ sensor that elicited changes in FRET upon activation both *in vitro* and in cells (23). This PKCα flanking sensor (50 nM) showed enhanced FRET upon activation with Ca^{2+} and liposomes containing DAG and PS (Fig. 1*b*; see "Experimental Procedures"). To address the possibility that the observed increase in FRET is primarily driven by confined localization on the lipid surface, the effect of Ca^{2+} and PMA, which is a soluble effector (24), was measured with similar results (Fig. 1*b*). The observed increase in FRET can arise from conformational changes within the PKC molecule or interactions between PKCs. GSG linkers inserted between PKCα and the two fluorophores (mCer and mCit) were designed to make the FRET readout sensitive to changes in distance rather than orientation of the two fluorophores. The current model of PKCα activation anticipates an increase in N- to C-terminal distance (18) and, therefore, is in contrast with the observed increase in FRET. To address whether intermolecular interactions contributed significantly to the observed FRET response, we generated a second, bimolecular FRET reporter system (mCer-PKCα-FLAG and PKCα-mCit-FLAG). Upon the addition of Ca^{2+} and liposomes containing DAG/PS, Ca^{2+} and PMA, or Ca^{2+} alone a significant increase in FRET was observed compared with the sensors in their basal state, consistent with an intermolecular interaction (Fig. 1*c*). The observed increases in FRET with the bimolecular FRET reporter are significantly higher than that due to cross-excitation of the acceptor (mCit). The effects of cross-excitation were determined by summing the spectra of samples with only mCer-PKCα (*light blue*) and only PKCα-mCit (*yellow*) (Fig. 1*c*; combined spectrum, *dashed line*). To assess what aspects of these observed increases in mCit/mCer occur from non-intended effects on the fluorophores and/or clustering of the proteins, we generated an additional bimolecular FRET reporter system containing the C2 domain of PKCα with mCit or mCer (residues 185–292). At equal molarity of each fluorophore, the ratio of mCit/mCer was assessed for both of the bimolecular FRET reporter systems basally, with Ca^{2+} and DAG/PS or with Ca^{2+} and PMA (Fig. 1*d*). Basally, both reporters display equivalent low/negligible levels of FRET, but PKC effectors increase FRET for the sensors containing full-length PKCα compared with the controls with only the C2 domain. Of note, the C2 domain sensors displayed a substantial increase in FRET in the condition with liposomes, which could be explained by a specific interaction between C2 domains in the presence of both of its cofactors Ca^{2+} and PS or from the local confinement of the sensors in a PS- and DAG-rich microdomain that forms in liposomes in the presence of Ca^{2+} (25).

As an orthogonal approach to FRET, a cross-linking assay was used. It has been previously reported that incubation of activated PKCα with a Cys-Cys cross-linker (BMH; 1.3-nm spacer arm) elicits an SDS-PAGE gel shift consistent with dimer formation (20). This result was reproducible with enrichment of cross-linked protein on Coomassie-stained SDS-PAGE gels between 170 and 250 kDa accompanied by loss of monomer (75 kDa) after effector stimulation of PKCα-FLAG (Fig. 1*e*). Although a consistent, single, higher molecular mass band between 170 and 250 kDa was always observed in experiments, the relative partitioning between monomer and cross-linked protein was variable between protein preparations and experimental repeats. Hence, cross-linking results were only compared within each experiment with matched controls. To probe for additional bands on the SDS-PAGE gel after cross-linking with increased sensitivity of detection, gels were transferred to a PVDF membrane and probed with a PKCα antibody (Fig. 1*f*). Increasing levels of a single cross-linked band were observed with Ca^{2+}, Ca^{2+} and PMA, and Ca^{2+} and DAG/PS (Fig. 1*f*). The band is consistent with PKCα-FLAG running between the expected molecular weight of dimeric and trimeric PKCα. A recent report used a similar Cys-Cys cross-linking assay (26) for the PKC-related protein (PRK) kinase and observed a homodimer running above its expected molecular weight. Based on this previous observation and the presence of a single higher molecular weight band, PKCα likely homodimerizes rather than forms a higher order oligomer.

The extent of cross-linking is independent of the concentration of PKCα-FLAG above concentrations of 100 nM (Fig. 1*g*). This observation is not consistent with clustering or crowding of PKC on membranes wherein increasing PKC concentrations with a constant concentration of lipids should increase cross-linked product (Fig. 1*g*). Importantly, an *in vitro* membrane localization assay shows that PKCα does not saturate the fixed concentration of lipids until >800 nM PKCα is added (Fig. 1*g*, *bottom panel*). As an additional control, a C619A mutant of PKCα-FLAG does not cross-link despite its ability to co-sediment with liposomes as well as the WT protein. Homodimerization of active PKCα has been previously suggested (11, 20, 27, 28) and together our *in vitro* observations, including the increase in FRET upon activation of the initial unimolecular sensor, are consistent with the formation of homodimer.

Functional Characterization of PKC Sensors—The addition of fluorophores and other modifications to PKCα did not compromise the basic enzymatic and processing functions of the WT protein. Several characteristics of PKCα including a single band on SDS-PAGE matching its expected molecular mass, priming phosphorylations at the hydrophobic motif (Ser(P)-657) and turn motif (Thr(P)-638) (29), and PKC effector-sensitive kinase activity support this observation (Fig. 2, *a–d*) (30). Of note we found that three commonly used PKC phosphorylation substrates, histone IIIs, MBP, or a peptide corresponding to residues 4–14 of MBP (MBP pep) at equal molarity elicited dramatically (roughly 1 order of magnitude) different ATPase activities of PKCα (Fig. 2*d*). We found that PKCα-FLAG and mCer-PKCα-mCit-FLAG behaved interchangeably in the ATPase assays (Fig. 2*e*). However, the PKCα-ΔC-tail-mCit-FLAG sensor used in Fig. 6, *a* and *c*, lacks the priming phosphorylations and, as previously reported (31), has no detectable ATPase activity. To assess if this sensor retains any of its native tertiary structure in the catalytic domain and as such can provide useful information on the binding interface, we adopted an assay that has commonly been used to measure nucleotide binding in other ATPases, including in protein kinase A (32), but has to our knowledge not been tested with PKCs. MANT-

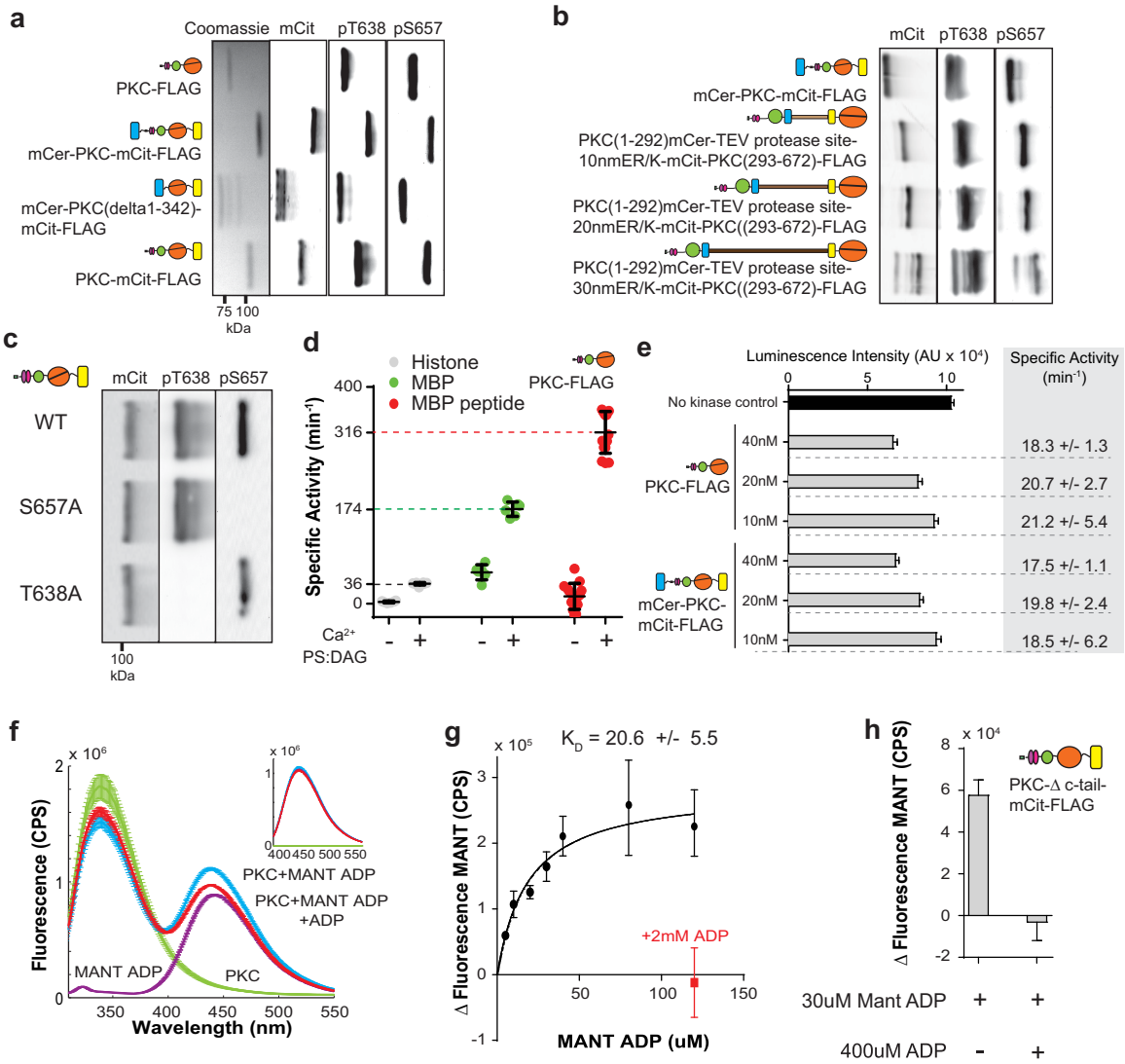

FIGURE 2. **Characterization of PKCα sensors.** *a–c*, sensors were analyzed for expected protein size and priming phosphorylation levels at the turn motif (Thr-638) and hydrophobic motif (Ser-657) sites assessed by immunoblotting with phospho-specific antibodies. Representative blots of PKCα-FLAG, mCer-PKCα-mCit-FLAG, mCer-CD-mCit-FLAG (*a*), RD- *n* nm SPASM- CD ($n = 10$, 20, or 30) (*b*), and PKCα-mCit-FLAG WT, T638A and S657A (*c*) are shown. *d*, specific activities of PKCα-FLAG with equimolar concentrations (20 μM) of three different phosphorylation substrates, histone IIIs, MBP full-length, and MBP peptide (residues 4–14). In each case a substantial increase in specific activity was observed after the addition of 750 μM $CaCl_2$ and ~80 μg/ml PS rich brain polar lipid extract (porcine) mixed with 2% w/w DAG. The means and S.E. of $n = 6–18$ reactions are reported. Negligible ATPase activity was observed in the absence of any phosphorylation substrate (data not shown). *e*, ATPase activity for the indicated concentrations of PKCα-FLAG and mCer-PKCα-mCit-FLAG in matched reactions with histone IIIs (12.5 μM) for 5 min. Raw data of luminescence intensity (proportional to residual ATP concentration at the end of the assay) was from the Kinase-Glo assay (Promega). Four independent reactions are shown with the means and S.E., and the calculated specific activities are shown at the *right*. ATPase activity is comparable between both constructs, and neither was sensitive to changes in concentration from 10 to 40 nM. *AU*, arbitrary units. *f* and *g*, MANT-ADP can be used to detect nucleotide binding to PKCα. *f*, raw spectra of PKCα-FLAG (1 μM) alone (*green*), incubated with MANT-ADP (120 μM; *blue*), or MANT-ADP and ADP (400 μM; *red*), or MANT-ADP alone (*purple*) excited at 290 nm (*main*) or 340 nm (*inset*) all in the presence of 1.5 mM $CaCl_2$ and 3.2 μM PMA. *g*, the difference in MANT-ADP fluorescence at 450 nm with or without PKCα-FLAG (1 μM) in the presence of $CaCl_2$ and PMA as a function of increasing MANT-ADP concentration. Specificity of MANT-ADP binding was assessed by the addition of 2 mM ADP in the presence of 120 μM MANT-ADP (*red*). Data are fit to a One Site-specific Binding function (Prism) to generate the indicated K_D of MANT-ADP binding to PKCα-FLAG. *h*, C-tail-deleted sensors retain the ability to bind nucleotide. MANT-ADP binding (increase in fluorescence at 450 nm) to PKCα-ΔC-tail-mCit (300 nM) in the presence or absence of ADP (400 μM; MANT-ADP, 30 μM). Measurements are made in the presence of 750 μM $CaCl_2$ and ~80 μg/ml DAG/brain extract liposomes. *Error bars*, S.E., $n \geq 3$.

labeled ADP is postulated to be a resonance energy acceptor from fluorescing tryptophans in the ATPase domain only if it binds to the catalytic site (32). Enhanced MANT-ADP excitation (450 nm) was detected upon the addition of activated PKCα-FLAG, which could be quenched with an excess of unlabeled ADP (Fig. 2*f*). A titration of MANT-ADP was fit to a one site-specific binding function (Prism) to establish a binding affinity of 20.6 ± 5.6 μM (Fig. 2*g*), similar to previous reports of ADP binding affinities of 5.5 μM for the ribosomal protein s6 kinase (S6K) (33) and 9.0 μM for protein kinase A (32). Despite the loss of catalytic activity upon deletion of the C-tail, PKCα-ΔC-tail-mCit-FLAG retained its ability to bind MANT-ADP (Fig. 2*h*), suggesting retention of its native tertiary structure. This is not surprising when considering homologous kinases such as PDK1 that fold properly without having a C-tail and are capable of kinase activity after *trans* binding of the C-tail of another AGC kinase (34). Taken together, these assays provide a toolbox for assessing the functionality of PKCα-derived sensors.

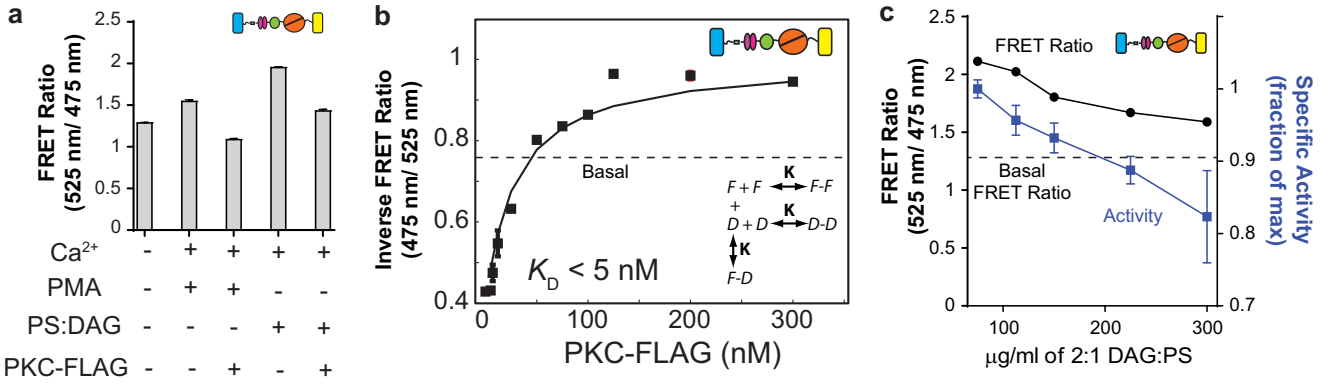

FIGURE 3. **Affinity of the homodimer interaction and its effect on kinase activity.** *a*, increased FRET ratio can be quenched by the addition of non-fluorescent PKCα. The FRET ratio of mCer-PKCα-mCit-FLAG (50 nM) with the indicated effectors with and without PKCα-FLAG (200 nM) is shown. *b*, competitive inhibition of PKCα dimerization can be used to estimate equilibrium dissociation constant (K_D). Increasing concentrations of PKCα-FLAG quench FRET levels of activated mCer-PKCα-mCit (Ca^{2+}+PS/DAG). Data are represented as inverse FRET ratio (475 nm/525 nm). ↑ Inverse FRET ratio = ↓ FRET. Equilibrium equations (*inset*) were fit to data to calculate a $K_D < 5$ nM. *c*, specific activity correlates with the extent of dimer formation. FRET levels (*black*; *left y* axis) and specific activity (*blue*; *right y* axis) of mCer-PKCα-mCit with increasing lipid concentration ($R^2 = 0.91$). *Error bars*, S.E. $n \geq 3$.

Estimate of PKCα Homodimer Binding Affinity and Effects on Specific Activity—The critical concentration at which dimerization of PKCα is observed is beyond the limit of both the bi-molecular FRET and cross-linking assays used in Fig. 1. Hence, a bimolecular FRET competition assay was utilized to estimate the binding affinity of a homodimeric PKC complex. The increased FRET for the mCer-PKCα-mCit-FLAG with the addition of Ca^{2+} and PMA or the addition of Ca^{2+} and PS/DAG can be competed off by the addition of PKCα-FLAG (Fig. 3*a*). By titrating PKCα-FLAG into a mixture of PS/DAG-activated mCer-PKCα-mCit-FLAG, the FRET was systematically quenched to below basal levels (Fig. 3*b*). The decrease in FRET does not stem from saturation of the liposomes, as the total PKCα concentration is well below the saturation limit determined in Fig. 1*g*. The competitive FRET inhibition was fit to an equilibrium partitioning between the three species (see "Experimental Procedures") to yield an upper bound on the bimolecular dissociation constant (K_D) of 5 nM. Of note, it was previously observed that the specific activity of PKCα increased *in vitro* at concentrations above 4 nM (11). To investigate the sensitivity of specific activity of mCer-PKCα-mCit-FLAG to the dimeric state, a fixed concentration of sensor was mixed with increasing concentrations of PS/DAG liposomes. Across a range of 80–300 μg/ml liposomes, a modest decrease in FRET and a correlated decrease in specific activity was observed (Fig. 3*c*; $R^2 = 0.91$). These results are consistent with a previous report that systematically demonstrated that the specific activity of PKCα is sensitive to its dilution across lipid vesicles (35). Higher liposomal concentrations did not allow for robust FRET measurements in our assays due to high light scattering from the lipids.

FRET Increase from mCer-PKCα-mCit-FLAG Is Observed upon PMA and LPA Activation in Live Cells—The flanking FRET sensor (mCer-PKCα-mCit-FLAG) was stably expressed in CHO cells to ~8-fold above endogenous PKCα levels (data not shown). The sensor basally resided in the cytosol and, consistent with previous studies using (N-terminal) eGFP-tagged PKCα, translocated to the plasma membrane after stimulation with PMA (Fig. 4, *a* and *c*), effectively mimicking the canonical response for PKCα (36). The basolateral membrane of the cell was imaged to provide a larger surface area for integration of FRET levels. The mean pixel-by-pixel FRET ratio increased steadily for the first 3 min post PMA stimulation and remained elevated through 15 min of imaging (Fig. 4*b*; *black*). As a control, DMSO treatment did not induce translocation or significant changes in FRET (Fig. 4*b*). As an orthogonal approach to measure FRET (17), the FRET response to the addition of PMA was determined using a live cell suspension in a spectrofluorometer (Fig. 4*b*, *green*). A substantial increase in FRET was observed after PMA addition, with a peak at 4 min, after a gradual decrease to basal levels within 8 min (Fig. 4*b*, *green*). Together, our measurements suggest that cellular activation of mCer-PKCα-mCit-FLAG by PMA causes an increase in FRET, but cell physiology plays a role in the persistence of the FRET response past the initial activation. A typical time-lapse of the accumulation of fluorescence at the basolateral membrane post PMA stimulation is shown (Fig. 4*c*) as well as a deconvolved Z-stack of the same cells at the 16-min time point (Fig. 4*d*). Most of the fluorescence accumulates at the plasma membrane, although a small fraction accumulates in the cytosol and nucleus consistent with results reported in NIH 3T3 cells (37). CHO cells stably expressing the sensor protein elicit a characteristic downstream PMA response by phosphorylating ERK1/2 (Fig. 4*e*). The PMA-dependent ERK1/2 phosphorylation persists >30 min after stimulation (Fig. 4*e*). The PMA-stimulated ERK1/2 phosphorylation is dependent on PKC activity, as it is abolished by the PKC-specific inhibitor BimI (1.5 μM) (Fig. 4*f*).

PMA activates PKC directly by binding its C1 domains (38). As a physiological stimulus, LPA was used to stimulate PKC as previously demonstrated (39). Unlike PMA, LPA elicits the characteristic membrane translocation response in only ~50% of the cells, consistent with previous reports (40). A transient PKC translocation to the plasma membrane was observed after LPA stimulation (Fig. 5*a*). Membrane translocation was accompanied by a transient increase in FRET for mCer-PKCα-mCit-FLAG (Fig. 5, *a* and *b*). The sensor protein also induced a biphasic ERK1/2 phosphorylation response with a dramatic increase at 2 min post stimulation and return to basal levels at 4

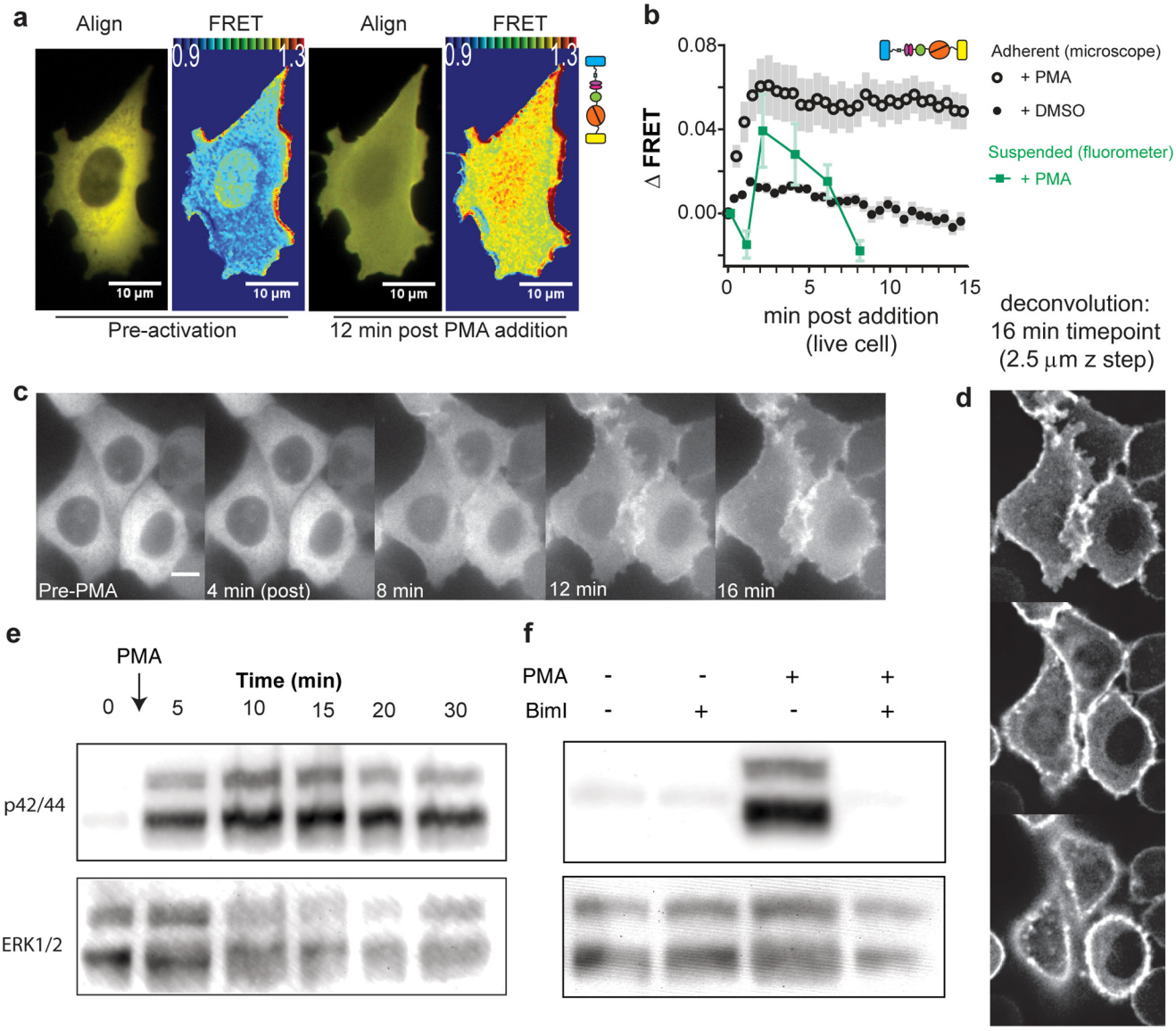

FIGURE 4. **FRET increase and ERK1/2 phosphorylation are observed in CHO cells following PMA stimulation.** *a–c*, PMA stimulation induces membrane translocation and increased FRET. *a*, representative image of a CHO cell stably expressing mCer-PKCα-mCit-FLAG before and 12 min after PMA stimulation (10 μM). *Align* is the alignment of the FRET donor (*green*) and FRET acceptor (*red*) channels. *FRET* is the pseudocolored pixel-by-pixel ratio of FRET acceptor to donor channel intensities using the indicated heat map. The microscope was focused on the basolateral cell membrane, where the fluorescent protein accumulates upon PMA stimulation. This method was chosen as a means to provide a larger surface area to integrate FRET ratios compared with the peripheral accumulation of fluorescence observed in a cross-sectional view of the cell (*d*). *b*, shown is the change in FRET in individual adherent cells by microscopy (*open black circles*) or suspended cells by spectroscopy (*green squares*) as a function of time post addition of PMA or DMSO control (*closed black circles*). For microscopy, results are the mean ± S.E. from 6–8 independent experiments ($n > 51$ cells). For spectroscopy, results are the mean ± S.E. of $n \geq 3$ independent experiments. *c*, representative time course of PMA stimulation images of CHO cells stably expressing mCer-PKCα-mCit-FLAG (mCit fluorescence). *Scale bar*, 10 μm. *d*, PKC translocates primarily to the plasma membrane with residual localization in the cytosol, nucleus, and cellular punctae. Shown are deconvolved images of the 16-min time point (*c*) at three different z-sections (2.5 μm apart). *e* and *f*, PMA stimulates PKC specific phosphorylation of ERK1/2. *e*, representative blot of the phosphorylation status of ERK1/2 in the same cell line (*a*) after the addition of PMA (1.92 μM) at the indicated time points. *f*, representative blot of ERK1/2 phosphorylation before or 15 min after PMA stimulation in the presence or absence of the PKC specific inhibitor BimI (1.5 μM).

min followed by sustained increase at 6 and 8 min (Fig. 5*c*). The persistent ERK1/2 phosphorylation 15 min post LPA treatment was inhibited by pretreatment with the PKC inhibitor BimI (Fig. 5*d*). We speculate that the biphasic ERK1/2 response to LPA is caused by bifurcation in LPA-induced PKC signaling with reconvergence of the signals at the downstream ERK1/2 at different time scales. Together, the LPA and PMA responses are consistent with mCer-PKCα-mCit-FLAG reporting an activated dimeric state for PKCα, consistent with our *in vitro* observations. However, other factors including clustering of the sensor at the plasma membrane or conformational changes independent of homodimerization may also contribute to the observed cellular FRET response after PKC activation.

Elements in Both the RD and CD Are Critical for Homodimerization—To identify the domains contributing to homodimerization *in vitro*, several domain truncations were made into the bimolecular FRET reporter system (mCer-PKCα-FLAG + PKCα-mCit-FLAG). It was observed that deletion of either both of the C1 domains or the conserved C-terminal extension of the AGC kinase domain (C-tail (V5)

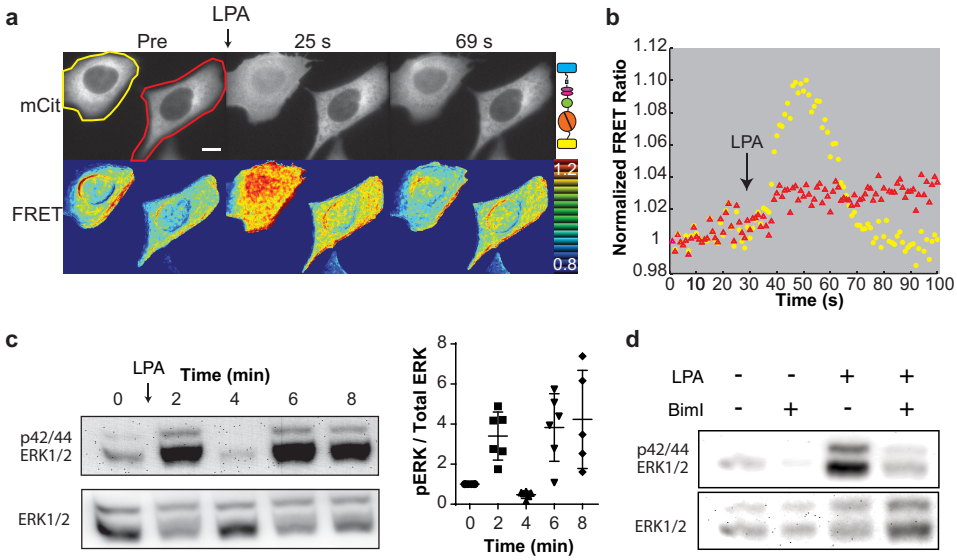

FIGURE 5. **FRET increase and ERK1/2 phosphorylation are observed in CHO cells following LPA stimulation.** *a* and *b*, concurrent transient membrane translocation and FRET increase after LPA (50 μM) stimulation. *a*, *top*, representative images of CHO cells with stable expression of mCer-PKCα-mCit. Translocation of the sensor from a diffuse cytosolic distribution (pre) to an accumulation on the basolateral membrane (25 s post LPA), which dissipates over time (69 s), depicts the canonical PKC response to activation. As would be expected based on previous observations (40), ~50% of the cells show the characteristic membrane translocation response after LPA stimulation. *Bottom*, FRET measurements are depicted as a heat map in corresponding images. *Scale bar* = 10 μm. Data are representative of $n >$ 25 cells. *b*, FRET ratio for cells in *a*. FRET ratios are normalized to the value at $t = 1$ s and adjusted for photo bleaching. *c*, biphasic ERK1/2 response to LPA stimulation. Shown is a representative blot and quantification of $n \geq 5$ independent replicates of ERK1/2 phosphorylation after LPA treatment (10 μM). *d*, representative blot of ERK1/2 phosphorylation before or 15 min after LPA stimulation in the presence or absence of the PKC-specific inhibitor Biml (1.5 μM).

domain) completely abolished the effector induced increase in FRET, whereas the deletion of the C2 domain retained a partial response (Fig. 6*a*). The involvement of the C1 and C2 domains in homodimerization is consistent with a previous report of a high affinity interaction between C1 and RD after activation (11). To probe for individual interactions between RD and CD (RD-RD, RD-CD, CD-CD), bi-molecular FRET pairs containing only the RD or CD were engineered. Although these confirm an enhanced RD-RD interaction (Fig. 6*b*), no appreciable interaction involving the CD (RD-CD, CD-CD) were detected upon activation even at concentrations much higher than the K_D (150 nM). These latter observations are in contrast with the effects of C-tail truncations in the context of full-length PKCα (Fig. 6*a*). The C-tail-truncated catalytic domains retain their ability to bind nucleotide, attesting to the retention of a folded catalytic site (Fig. 2*h*). The C-tail is a conserved region of the kinase domain that is required to stabilize the active state of the kinase and is critical for hetero-dimerization of almost all AGC kinases (41). An alternative interpretation for the lack of FRET response for the C-tail deletion sensor is the displacement of the C-terminal mCit fluorphore such that no FRET is detected despite the occurrence of homodimerization. To test this possibility, a second bimolecular FRET pair (mCer-PKCα-FLAG + mCit-PKCα-FLAG) was tested. The increase in FRET upon activation was found to be independent of which termini the fluorophores are positioned on PKC (Fig. 6*c*). The C-tail involvement in homodimerization was confirmed by an almost complete loss of FRET after deletion of only one C-tail in either of the bimolecular FRET pairs (mCer-PKCα + PKCα-ΔC-tail-mCit; mCer-PKCα-ΔC-tail + mCit-PKCα) (Fig. 6*c*). Together, these observations suggest that intermolecular interactions involving both the RD and CD contribute to homodimerization.

SPASM Technique Demonstrates That the RD and CD Interact in the Dimeric State—In the context of the intact PKC protein, all domains are tethered in close spatial proximity, which increases their local effective concentration. Hence, weak interactions between domains (RD-CD, CD-CD) that are nonetheless essential for homodimerization may not be detected in bimolecular assays. To address this limitation, SPASM modules were spliced into different locations of full-length PKCα. The SPASM module consists of a FRET pair (mCit/mCer) flanking an ER/K linker, which controls the effective concentration of the interaction between proteins fused to its ends (10). These modules are designed to (*a*) artificially increase the local concentration of domains as compared with untethered domains while (*b*) using the FRET readout to resolve effector-stimulated changes in interactions between domains. Given that the bimolecular RD-RD interaction is enhanced after PKC activation (11), it can serve to nucleate additional RD-CD and CD-CD interactions. Thus, a SPASM module was spliced in between the RD and CD to test for an intermolecular RD-CD or CD-CD interaction that can stabilize a high affinity dimer. To avoid potential complications from intramolecular interactions, a 30-nm ER/K linker was used (low effective concentration of the intramolecular interaction (10)), and the system was engineered to report only on bimolecular interactions (FRET donor placed adjacent to either the RD or CD; FRET acceptor adjacent to the CD of a different sensor). Both sensor pairs showed a comparable increase in FRET upon activation providing direct evidence for a RD-CD interaction, with the potential for a CD-CD interaction in the homodimeric state (Fig. 6*d*). Next, a 10-nm SPASM module was inserted in three separate locations in the PKC gene (*1*, between the pseudosubstrate (PS) and C1a domain; *2*, between the C1b and C2 domains; *3*, between the C2

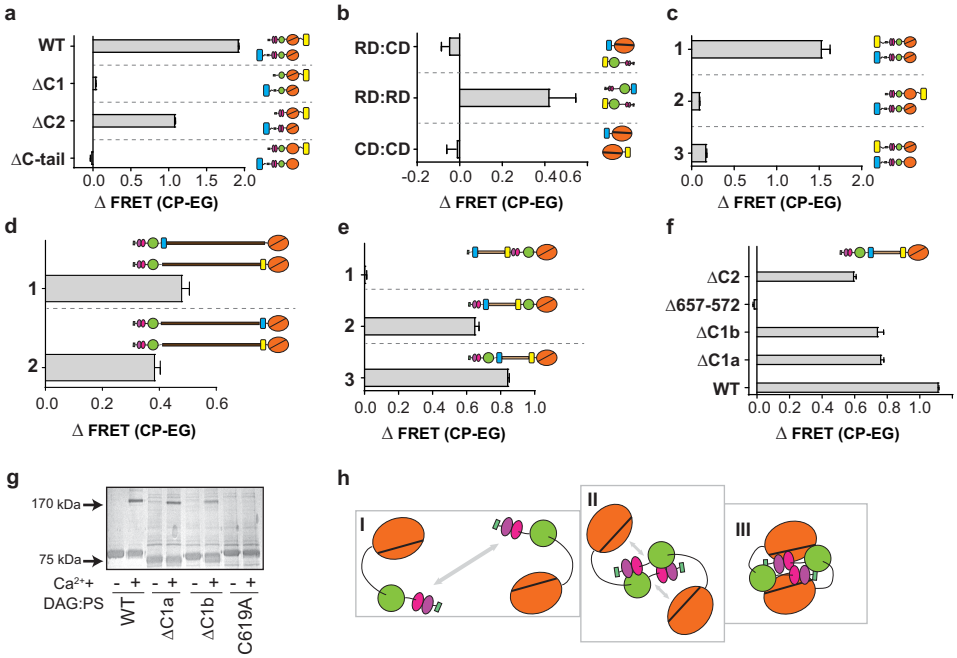

FIGURE 6. **Conformation of the PKC homodimer.** *a–d*, change in FRET ratio (Δ*FRET*) from basal (EGTA (*EG*)) to activating (Ca^{2+} + PMA (*CP*)) conditions for the indicated sensors. *a–d*, FRET donor and acceptor are on different sensors. An increase in FRET indicates an intermolecular interaction. *e* and *f*, FRET donor and acceptor are on the same sensor but separated by an ER/K linker. In the absence of an interaction, the 10-nm ER/K linker separates domains beyond FRET distance. An increase in FRET indicates enhanced interaction between domains at either end of the ER/K linker. *a*, C1 and C-tail domains are essential for PKCα homodimerization; mCer-PKCα + PKCα-mCit with no truncation (*WT*) or ΔC1, ΔC2, ΔC-tail in both proteins. *b*, a bimolecular RD-RD interaction, but not an RD-CD interaction or CD-CD interaction is detected after activation. *RD-CD*, mCer-CD + mCit-RD; *RD-RD*, mCit-RD + mCer-RD; *CD-CD*, mCer-CD + mCit-CD (50 nM donor sensor, 100 nM acceptor sensor). *c*, the C-tail in the catalytic domain is essential for homodimerization. *1*, mCer-PKCα + mCit-PKCα; *2*, mCer-PKCα + PKCα-ΔC-tail-mCit; *3*, mCer-PKCα-ΔC-tail + mCit-PKCα. *d*, both the RD and CD domains reside at the dimerization interface. *1*, RD-mCer-30-nm ERK-CD + RD-30 nM ERK-mCit-CD; *2*, RD-30-nM ERK-mCer-CD + RD-30-nm ERK-mCit-CD. *e*, enhanced RD-CD interaction in the PKC homodimer. *1*, PS-mCer-10-nm ERK-mCit-C1-C2-CD; *2*, PS-C1-mCer-10-nm ERK-mCit-C2-CD; *3*, RD-mCer-10-nm ERK-mCit-CD. *f*, C1a, C1b, and C2 domains partially contribute to dimerization, whereas the C-terminal 15 residues of the C-tail are essential. Shown is change in FRET upon activation of type 3 configuration (as in *e*), with truncation of the C1a, C1b, C2 domains or the C-terminal 15 residues of the C-tail. *g*, proximity of the C-tail to the homodimer interface. Shown is a representative Coomassie-stained gel of PKCα-FLAG protein under basal or activated (Ca^{2+}+*DAG/PS*) conditions. Data for full-length PKCα (*WT*), domain deletions (Δ*C1a*, Δ*C1b*), and mutant (*C619A*) proteins are shown. Note the complete loss of detectable dimerization upon mutagenesis of a Cys-619 in the C-tail region of the CD. The BMH cross-linker has a maximal reach of 1.4 nm. For reference the C1b domain is about 3 × 2 × 2 nm (18). *h*, model for dimer formation based on data presented in *a–g*. *I*, RDs interact with each other upon effector stimulation to nucleate homodimerization. *II*, RD-CD interaction in *trans* facilitated by the C-tail. *III*, proposed conformation for the PKC homodimer. *a–f*, *error bars*, S.E. $n \geq 3$.

and CD). Although the PS is known to interact with the CD basally (42), this interaction did not change after activation (type 1; Fig. 6*e*). In contrast, the C1 domains display a marked enhancement in interaction with either the C2 or CD after activation (type 2), whereas collectively the RDs interact very prominently with the CD after activation (type 3; Fig. 6*e*). Using the type 3 configuration to directly report on the interaction between the RD and CD, deletions of C1a, C1b, C2, or the C-terminal 15 residues of the C-tail were made. Surprisingly, the activated RD-CD interaction remained partially intact after the deletion of any of the three regulatory domains, but shortening of the C terminus of the C-tail completely disrupted this interaction (Fig. 6*f*). Together, these data suggest that all three regulatory domains (C1a, C1b, and C2) contribute to the dimer interface, but the C-tail is absolutely critical for the interaction. Given that the C-tail is essential for the active conformation of the kinase domain (43), these data cannot distinguish between a direct role for the C-tail as part of the dimerization interface and its indirect contribution through the global conformation of the kinase domain.

To probe for precise interfaces involved in homodimerization, we sought to identify Cys residues that were being cross-linked by BMH, which requires two Cys residues to be within 1.3 nm. The only Cys residues within PKCα are found in the Cys-rich C1a and C1b domains and within the CD. Activation-specific cross-linking was still detected after deletion of either the C1a or C1b, yet a single point mutation in the C-tail (C619A) completely abolished the cross-linking response (Fig. 6*g*). Interestingly, the corresponding residue in PKCβII (Cys-622), which is found in the active-site tether region, is buried within an interaction interface with the C1b domain in a recent crystal structure (18). This raises the possibility that the interaction between the C1b and c-tail captured in the crystal structure could be an interaction utilized in dimerization. Regardless, our data propose a new conformation for activated PKC wherein the CD, C1a, C1b, and the C2 domains all contribute to stabilizing a homodimer (Fig. 6*h*). It was reported from two separate groups that truncation of the C-terminal 10 residues in the C-tail (31) or alanine mutagenesis of regions from the C1a and C2 domains (44) completely abolished activity of PKCα. A potential explanation for these observations is the disruption of homodimerization and its consequent effects on PKC catalytic activity. To probe the function of a homodimeric conformational state, we report on four independent vignettes concerning different aspects of PKCα function. Each provides some insight and highlight how our mechanistic understanding of PKCα function is enhanced when considering this additional state.

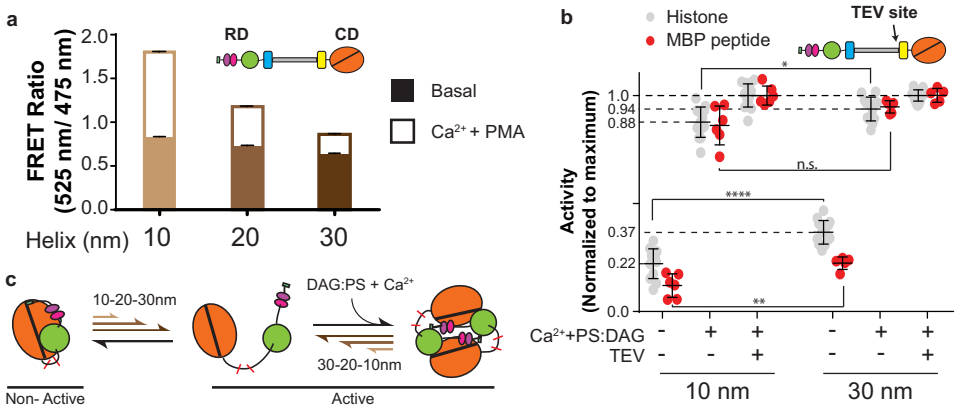

FIGURE 7. **Dimerization facilitates high kinase activity through disruption of auto-inhibition.** *a*, effector binding and not disruption of the RD-CD interaction is necessary for homodimer formation. Perturbation of the basal RD-CD interaction with an ER/K linker does not induce dimerization. The basal (*solid*) and activated (*hollow*) FRET ratio of three PKC reporters with 10-, 20-, and 30-nm SPASM modules inserted between the RD and CD (between Glu-292 and Gly-293). All three sensors have increased FRET after the addition of Ca^{2+} + PMA. *b*, disruption of the basal RD-CD interaction only modestly increases specific activity. The activity of the 10- and 30-nm sensors (80 nM) under the indicated conditions with histone IIIs (*gray*) or MBP peptide (*red*) as substrate is shown. TEV treatment cleaves a specific site engineered at the N terminus of the ER/K linker separating the RD from the CD. TEV treatment followed by the addition of Ca^{2+} and DAG/PS yields maximal activity of the catalytic domain due to membrane partitioning of the RD and soluble partitioning of the CD. The basal activity but not the activity in the presence of effectors was significantly enhanced when increasing the SPASM module length from 10 to 30 nm (Student's *t* test 99% confidence interval: *p* values for not significant (*ns*) = 0.073; * = 0.0212; ** = 0.0042, **** < 0.0001). *a* and *b*, *error bars*, S.E. $n \geq 3$. *c*, schematic of the effect of the different length ER/K linkers on the three-state equilibrium for PKCα.

Equilibrium between Closed, Open, and Dimerized Conformations of PKCα—In the absence of effectors PKCα predominantly populates a "closed" conformation with the CD auto-inhibited by the RD (18). Splicing a SPASM module between the RD and CD should decrease the effective concentration of the RD for the CD in proportion to the length of the linker. "Prying" open the RD-CD interaction with SPASM modules containing increasing-length ER/K linkers systematically reduces the basal level of FRET (Fig. 7*a*) and increases the basal level of activity (Fig. 7*b*; 10 nm, ~22/12%; 30 nm, ~37/22% maximum activity, compared with ~3/3% for WT PKCα (histone IIIs/MBP pep)). Of note, prying open the RD-CD interaction alone is not sufficient to induce dimerization in the absence of effectors. Yet the presence of effectors increases FRET regardless of ER/K linker length (Fig. 7*a*). Given the importance of RD-CD interactions for dimer formation (Fig. 6), it is not surprising that increasing ER/K linker length also disrupts dimer formation (Fig. 7*a*). Despite the different levels of FRET with 10- and 30-nm ER/K linkers after activation, they both have specific activity similar to that of the CD in the absence of the RD (TEV cleaved) (Fig. 7*b*; 10 nm, ~88/86%, 30 nm, ~94/95% maximum activity (histone IIIs/MBP pep)). Following TEV treatment the RD should partition to the lipid vesicles leaving the CD completely uninhibited. It was observed that in the presence of effectors both the 10 and 30 nm ER/K linkers demonstrate similar activities despite different levels of FRET. Taken together these results are consistent with a dynamic equilibrium for PKCα between a closed (basal auto-inhibited: medium/low FRET), an open (no auto-inhibition: low FRET), and a dimeric conformation (no auto-inhibition: high FRET) with equivalent specific activities in the open and dimer forms (Fig. 7*c*). In the proposed model for mature PKCα, the specific activity is regulated by only one parameter, namely, the ratio of non-auto-inhibited catalytic domains to the total number of catalytic domains in a given reaction.

Loss of the Turn Motif Priming Phosphorylation Causes Basal Dimerization—We next aimed to bridge our global structural model of PKC to high resolution x-ray crystallographic data. A recent partial crystal structure of PKCβII suggests a direct binding interaction between its C1b and C-tail domains (18). To investigate the possibility that this interaction is similar to the one utilized in homodimerization of PKCα, individual point mutations in PKCα (K621A, D357A, H633G, T638A) were engineered in an attempt to disrupt the C1b-C-tail interaction. The residues are mapped onto the crystal structure of PKCβII (orange surface rendering) as well as Cys-619 (*yellow surface rendering*) for visual reference (Fig. 8*a*). Each mutation engineering into the bimolecular FRET reporters elicited modest effects, except for T638A, which counter intuitively increased the FRET response under basal and effector-stimulated conditions (Fig. 8, *b* and *c*). Cross-linking analysis of the T638A mutant confirmed the basal formation of a dimeric species (Fig. 8*d*). Residue Thr-638 is an essential priming phosphorylation site (turn motif (TM)) in PKCα that is essential for full catalytic activity after activation (45). The T638A mutant has ~36/22% (histone/MBP pep) of WT PKCα activity after activation with Ca^{2+} + PS/DAG (data not shown), similar to previous reports (45). The Thr → Ala mutant is commonly incorporated in the TM site to mimic the loss of TM site phosphorylation (45–47). Using such an approach for multiple AGC kinases including PKCζ, it has been broadly suggested that TM phosphorylation functions to anchor the C-terminal portion of the C-tail, containing the hydrophobic motif, to the catalytic domain (47). Based on this model, it might be anticipated that basal homodimerization of PKCα-T638A is the result of an indirect destabilization of the interaction of the catalytic domain with the phosphorylated hydrophobic motif site on the C-tail. To assess this possibility, phospho-null mutation of the hydrophobic motif site (S657A) was incorporated into the FRET sensors. In contrast with the

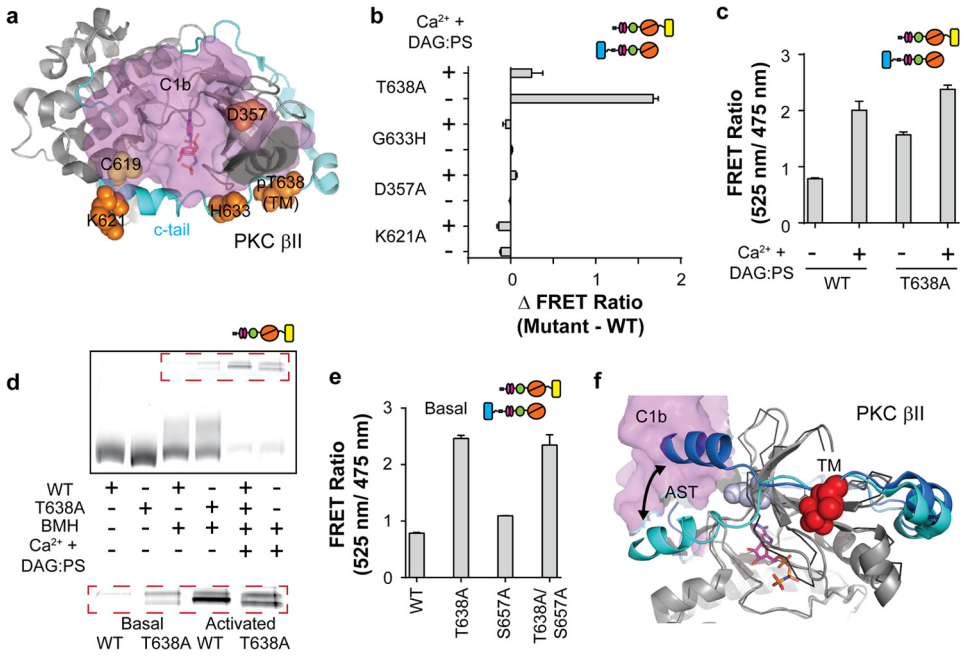

FIGURE 8. **Point mutation in the turn motif phosphorylation site causes PKCα to dimerize basally *in vitro*.** *a*, schematic of the interface between C1b (*magenta* surface contour) and the catalytic domain of PKCβII (PDB code 3PFQ) highlighting the c-tail (*cyan schematic*), the BMH cross-linked C619 (*yellow spheres*), and residues mutagenized (*orange spheres*). *b* and *c*, only T638A (turn motif) shows a substantial change in FRET compared with WT in both basal and effector-stimulated conditions when inserted into both mCer-PKCα-FLAG + PKCα-mCit-FLAG sensors. *d*, BMH cross-linking supports enhanced basal dimerization of T638A mutant. Wild type or T638A PKCα-mCit-FLAG cross-linking was assessed under the indicated conditions. The *inset* shows the contrast-adjusted intensity from the same gels. *e*, loss of turn-motif phosphorylation does not induce dimerization solely through allosteric changes in hydrophobic motif site. Basal FRET levels for WT, turn motif mutant (*T638A*), hydrophobic motif mutant (*S657A*), and double mutant (*T638A/S657A*) bimolecular FRET sensors (mCer-PKCα-FLAG + PKCα-mCit-FLAG) are shown. *f*, PyMOL-aligned crystal structures (PDB code 2I0E, *blue and black ribbon*; PDB code 3PFQ, *cyan and gray*) of the PKCβII catalytic domain highlighting the relative positions of the c-tail (615 - 669). The phosphorylated turn motif residue (T638; red spheres) interacts tightly with the catalytic domain through four conserved electrostatic interactions (in PKCβII K350, K355, K374, R415) that appear to serve as a fulcrum point around which conformational changes in the c-tail are centered.

proposed model, basal homodimerization induced by T638A is independent of the S657A mutation (Fig. 8*e*). The mechanism by which T638A induces basal dimerization is informed by an alignment of two crystal structures of the catalytic domain of PKCβII (Fig. 8*f*; Ref. 48). The region just N-terminal of the TM site (AST region; Ref. 43) undergoes a dramatic conformational change when bound to C1b (*cyan*), yet in both structures the C-tail converges at the phosphorylated TM residue that appears tightly anchored to the catalytic domain by electrostatic interactions with four basic residues (*red*) (Fig. 8*f*). We postulate that disruption of the anchoring phosphorylated TM site allows the AST region of the C-tail to adopt a conformation that can induce homodimerization in the absence of effectors. Independent of this interpretation, the finding that an unphosphorylated TM can basally homodimerize may provide a mechanism by which PKCα, unlike most AGC kinases, is autophosphorylated at its three priming sites (6, 49) and deserves further investigation.

Disruption of PMA/LPA-induced High FRET State in Cells Modulates PKC-specific Phosphorylation of ERK1/2—To test the functional significance of dimerization in cells, one peptide each from the RD and CD was selected to specifically disrupt (relative to a matched scrambled peptide; all myristoylated) prospective PKCα dimerization interfaces. Although the effects of the peptides on FRET were modest *in vitro*, they were specific and concentration-dependent across two different sensor systems (Fig. 9, *a* and *b*). Additionally, the RD peptide did not disrupt liposome binding in sedimentation assays (Fig. 9*c*). When treating cells with the myristoylated RD peptide, the PMA-induced high FRET state of mCer-PKCα-mCit-FLAG was disrupted in live cell suspensions (Fig. 9*d*; fluorometer measurements). Both the RD and CD peptides had a significant and sustained dampening effect on the PMA-induced increase in FRET of the sensor compared with their respective scrambled peptide controls (Fig. 9*e*; microscope measurements). Additionally, neither peptide had a noticeable effect on the rate or relative degree of basolateral membrane translocation of the sensor in CHO cells after PMA treatment (Fig. 9*f*; data not shown). Next, the effect the peptides had on the PMA- and LPA-induced phosphorylation of ERK1/2 was assessed by pretreatment of cells for 15 min before stimulation with PMA or LPA. The native RD peptide specifically lowered the level of ERK1/2 phosphorylation after PMA (Fig. 9*g*) or LPA treatment (Fig. 9*h*) relative to the scrambled control. When the cells were stimulated with serum, which is expected to activate ERK1/2 through both PKC-dependent and independent pathways (50), both the RD peptide and the known PKC inhibitor BimI had comparable partial effects (Fig. 9*i*). Last, the CD peptide was able to specifically disrupt LPA-induced ERK1/2 phosphorylation compared with its scrambled control (Fig. 9*j*). Together, these results are consistent with a model in which disruption of PKCα homodimerization is capable of inhibiting PKC-mediated downstream ERK1/2 phosphorylation.

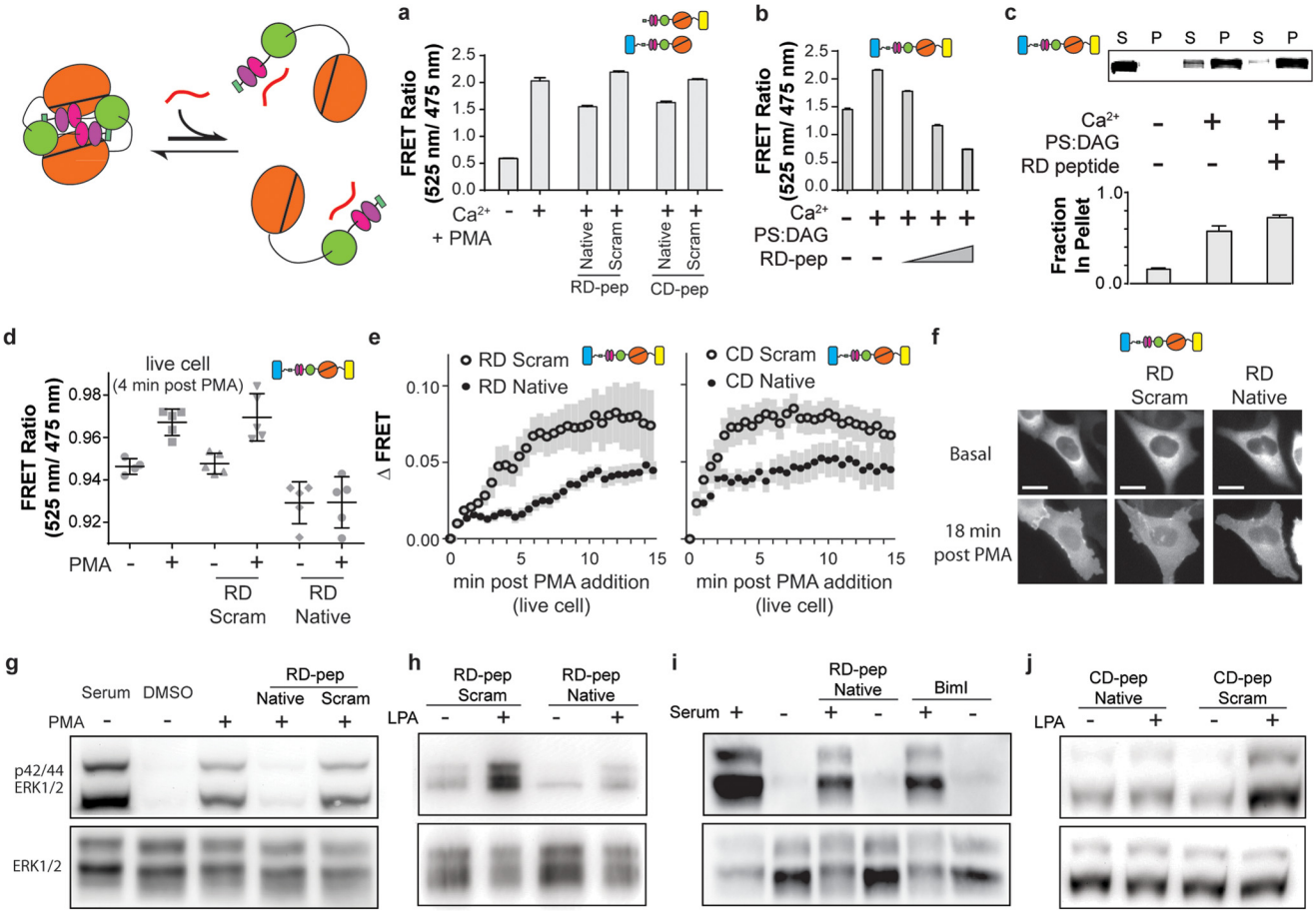

FIGURE 9. **Disruption of activation induced PKC sensor high FRET state in CHO cells modulates PKC function.** *a*, peptides from the RD and CD domains can disrupt dimerization in recombinant protein. Shown is the FRET ratio for mCer-PKCα (40 nM) combined with PKCα-mCit (160 nM) under the indicated conditions. *Ca^{2+}+PMA*, 1.5 mM $CaCl_2$ + 3.2 μM PMA. *RD-pep* and *CD-pep* are myristoylated peptides analogous to residues 218–226 in the regulatory domain and 633–642 in the catalytic domain. *Native*, native PKC sequence; *Scram*, matched scrambled sequence control. Peptides concentrations were 10 μM. *b*, peptides decrease FRET in a concentration-dependent manner. The *in vitro* FRET ratios of mCer-PKCα-mCit-FLAG with increasing concentrations of RD-pep (0, 10, 20, 50 μM) are shown. *c*, peptide does not alter membrane translocation of PKC. mCer-PKCα-mCit-FLAG was incubated with Ca^{2+} and sucrose-loaded PS/DAG vesicles with and without the native RD-pep, before ultra-centrifugation. After ultracentrifugation, the pelleted (*P*) and supernatant (*S*) fractions were run on an SDS-PAGE gel and scanned for mCit fluorescence. *Top*, a representative gel image; *Bottom*, quantification from three separate experiments. *d* and *e*, peptides suppress the characteristic increase in mCer-PKCα-mCit FRET after PMA stimulation in live cells. *d*, FRET ratio of suspended CHO cells (fluorometer detection) stably expressing mCer-PKCα-mCit-FLAG, pre- and 4 min post-10 μM PMA addition in the presence or absence of 20 μM concentrations of the indicated peptide. Maximum FRET was observed 4 min post-PMA stimulation (see Fig. 2*a*). *Error bars*, S.E. $n > 5$. *e*, microscope-based detection of changes in FRET ratio (Δ *FRET*) in adherent cells, preincubated for 15 min with the indicated peptides (10 μM) followed by stimulation with 10 μM PMA. *Error bars*, S.E. $n = 13–24$ cells. *f*, peptides do not influence membrane translocation of PKCα. Representative images of cells pre- and 18 min post-PMA addition. *Scale bars* = 10 μm. *g–j*, RD and CD peptides, but not matched scrambled controls, disrupt PMA or LPA-stimulated ERK1/2 phosphorylation. Peptides do not influence PKC-independent (serum)-driven phosphorylation of ERK1/2. Serum-starved CHO cells stably expressing mCer-PKCα-mCit-FLAG were preincubated with 20 μM concentrations of the indicated peptide (or 1.5 μM BimI) for 15 min before stimulation (10% serum, 10 μM LPA, or 1.92 μM PMA) and lysed 15 min post-stimulation. Representative Western blots of phospho and total ERK1/2.

Destabilizing the Closed Conformation Provides Stable PKCα Translocation to the Membrane—The PKC inhibitor GF109203x is known to stabilize the translocation of PKCα after effector stimulation (46). Stensman *et al.* (46) hypothesized that the mechanism of GF109203x-influenced translocation sensitivity is due to a destabilization of the basal RD-CD interaction. Additionally, several analogues of this inhibitor, including BimI, are known to induce conformational changes in the CD (51). Using a PKCα sensor with a SPASM module inserted between the RD and CD, we directly detect a reduction in the strength of the interaction between RD and CD when incubated with BimI under basal conditions (Fig. 10*a*). Based on the three-state model (Fig. 7*c*), destabilization of the closed conformation should drive the equilibrium toward dimer formation after effector stimulation. Accordingly, we find increased dimerization of PKCα in the presence of BimI (Fig. 10, *b* and *c*). We hypothesize that both the open and dimeric conformations of PKCα can engage with the plasma membrane. Consistent with this concept, LPA stimulation of cells stably expressing the flanking sensor (mCer-PKCα-mCit), substantially increased the fraction of cells with stable localization of the sensor at the membrane in the presence of BimI (Fig. 9, *d* and *e*). Our findings provide direct evidence that a small molecule that can destabilize the closed conformation can facilitate both dimerization and stabilize membrane localization of PKCα in the presence of effectors. This opens the possibility of other small molecules or interacting proteins influencing localization of PKC by influencing the stability of either the closed or dimer states. As a corollary, PKC translocation is not necessarily an

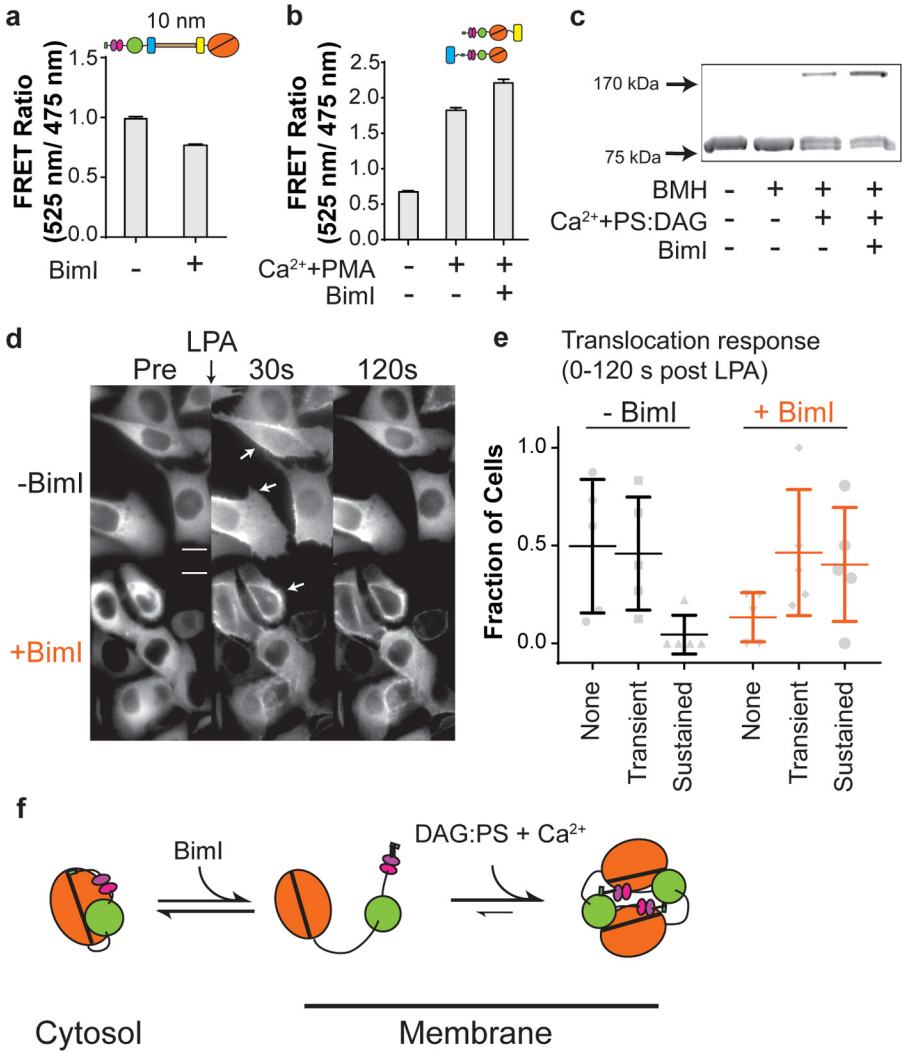

FIGURE 10. **Disruption of the auto-inhibited state prolongs translocation.** *a*, BimI (10 μM) destabilizes the auto-inhibited state. FRET ratio in the absence of effectors of sensor with a SPASM module inserted between RD and CD (between Glu-292 and Gly-293). *b* and *c*, BimI increases dimer formation after effector stimulation. *b*, FRET ratio for mCer-PKCα with PKCα-mCit. *c*, cross-linking analysis of PKCα-FLAG incubated with Ca^{2+} and PMA or Ca^{2+} and PS:DAG. *d* and *e*, BimI induces sustained translocation of PKCα. *d*, *top*, representative images of CHO cells stably expressing mCer-PKCα-mCit pre- and 30- and 120 s post-LPA (50 μM) stimulation. Two cells with transient translocation are highlighted (*white arrows*). Translocation was observed as either a ring of high intensity fluorescence or the appearance of fluorescence along the basolateral membrane of the cell. *Bottom*, representative images with the addition of 1.5 μM BimI 2 min before LPA stimulation. The *white arrow* highlights a cell with a sustained translocation response. *Scale bars* = 10 μm. *e*, translocation response in CHO cells stably expressing the mCer-PKCα-mCit sensor in response to LPA stimulation (50 μM) without or with 1.5 μM BimI pretreatment. Cells were binned as no apparent response (*None*), a transient translocation response (*Transient*, translocation occurs and recedes within 120 s), or a sustained translocation response (*Sustained*, translocation is still present after 120 s). Data points represent five independent experiments, ~20 cells per experiment. The fraction of the cells binned in each category for each experiment is plotted with a spread in the data indicated as the mean ± S.E. *f*, schematic illustrating the effect of BimI on the three-state equilibrium of PKCα.

appropriate proxy for PKC activation in live cells as demonstrated by the decoupling of activity and translocation with the peptide inhibitors (Fig. 9) and BimI (Fig. 10, *d* and *e*).

DISCUSSION

PKC, a Conservative and Dynamic Kinase—The negative consequences of unregulated PKC activity have been apparent since its discovery as the receptor for tumor-producing phorbol esters (38). In the subsequent decades it has been observed that the dysregulation of PKC function is tied with several different pathologies (52–55). Concurrently, multiple distinct mechanisms of auto-inhibition of PKC have been described (18, 42, 56, 57). Collectively these findings portray PKC as a conservative signaling protein that is only capable of functioning under a limited ensemble of conditions. In contrast, an increasing body of evidence positions PKC as a lynchpin in intracellular communication in diverse signaling environments (58). The mechanisms allowing PKC to transition from the tightly regulated auto-inhibited state to a catalytically active state in a dynamic manner and in the context of multiple signaling inputs have been largely unexplored. In this study we find that homodimerization is an additional regulatory mechanism exploited by PKCα to overcome intramolecular auto-inhibition.

Three-state Model—Our data confirm previous reports that find a positive correlation between PKC concentration or dimerization and specific activity (11, 20, 35) (Fig. 3*c*; data not shown). A possible explanation is that intermolecular interactions in the homodimer enhance the catalytic activity of the kinase domain. However, the fully activated homodimeric PKC

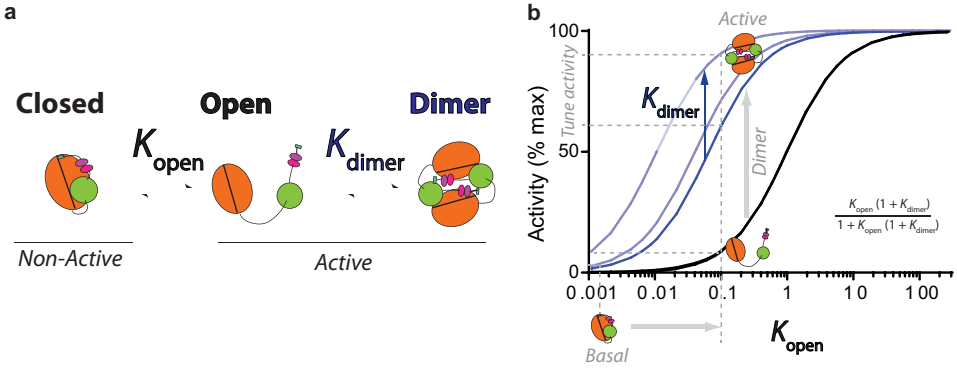

FIGURE 11. **Dimerization latches open the stimulated kinase.** Dimer formation allows for more specific activity from lower levels of effectors. *a*, PKC activation is modeled as a three-state (*closed*, *Open*, or *Dimer*) equilibrium with equilibrium constants K_{open} and K_{dimer}. *b*, the specific activity of PKC when the closed state is inactive and both the open and dimer state are fully active is plotted as a function of opening PKC ($\uparrow$ K_{open}). For a given potency of effectors in releasing PKC auto-inhibition (defined K_{open}), dimer formation can substantially enhance specific activity. Factors that control dimer formation (K_{dimer}), including local concentration of protein, co-factors, and small molecules, can tune local PKC activity over a wide range. The *black line* represents PKC with no ability to form a dimer, whereas the *blue lines* have increasingly higher values of K_{dimer}.

is less active (86%) than just the catalytic domain (Fig. 7). Furthermore, varying the fraction of activated PKC in the monomer and dimer states with different length ER/K helices between the RD and CD did not affect specific activity in the presence of effectors (Fig. 7). Orthogonally, it was observed that prying open the basal auto-inhibitory interactions using ER/K helices only modestly increased specific activity (Fig. 7). These observations lead us to propose a model wherein dimerization acts as a "mass action sink" by sequestering the regulatory domains away from their autoinhibitory interactions. In our proposed three-state model, PKC is in dynamic equilibrium between the auto-inhibited state that has no catalytic activity (0%), the monomeric and non-auto-inhibited (open) state that has full catalytic activity (100%), and the homodimeric state that also has full catalytic activity (100%). In Fig. 11 we use this model to demonstrate how dimerization can influence the specific activity of PKC. Of particular note in this three-state model there are now two largely independent ways in which PKC could be activated; through disruption of the auto-inhibitory interactions (K_{open}) or through stabilization of the homodimer (K_{dimer}). Likely, canonical PKC effectors, such as those used in this study, will modulate both equilibrium constants. We postulate that for the nuanced regulation observed in cells, interactions between PKC and small molecules or proteins may differentially influence these two parameters.

Peptides and Small Molecules Can Modulate PKC Function through Two Distinct Mechanisms—In this study we demonstrate the feasibility and physiological significance of peptide and small molecule modulation of intramolecular interactions in PKC. Two peptides were identified and characterized that selectively disrupt the homodimeric state (K_{dimer}) of PKC (Fig. 9, *a–f*). When introduced into a cellular system, both peptides specifically and dramatically reduced the PKC-driven downstream phosphorylation of ERK1/2 (Fig. 9, *g--j*). Conversely, we observed that the small molecule PKC inhibitor BimI disrupted the interaction between the auto-inhibited and open states (K_{open}; Fig. 10*a*), which in turn leads to an increase in the homodimeric state (Fig. 10, *b* and *c*). When introduced into a cellular system, BimI was able to alter the translocation response of PKC post LPA stimulation (Fig. 10, *d* and *e*). These results demonstrate potential approaches for PKC intervention as well as provide precedence and detailed mechanism for non-canonical PKC regulation that could be utilized in physiological contexts.

Dimeric State Versus Higher Order Oligomerization—Although the results presented here are consistent with homodimerization of PKCα, they do not rule out the formation of higher order oligomers. The FRET measurements do not differentiate between homodimers and higher order oligomers. However, the cross-linking studies show a single dominant higher molecular weight band that is consistent with a dimer. Given that BMH cross-linking is limited to the close proximity (1.3 nm) of two cysteines, it is possible that higher order oligomers are not efficiently cross-linked, resulting in dimerization as the predominant species detected using this method. With the absence of evidence for higher order oligomerization, we have presented concepts along the lines of the simplest oligomeric state (dimer). Notably, the concept of dimerization sequestering the regulatory domains away from the auto-inhibited state is compatible with higher order oligomerization. In regard to higher order oligomerization, it has been previously reported that PKC as well as certain PKC phosphorylation substrates can drive phase separation on lipid membranes (25). Additionally, the potent PKC activator protamine sulfate has been shown to aggregate PKC in an active state in the absence of additional effectors *in vitro* (59). Further studies are necessary to probe the possibility of higher order PKC oligomerization and its physiological relevance.

Domain-Domain Interactions in Other AGC Kinases—Interactions between modular domains are known to broadly regulate AGC kinases. However, none of them have been proposed to utilize the specific mechanism described here. The AGC kinase PDK1 is known to heterodimerize with several AGC kinases including PKCs, AKT, PKN, and S6K through interactions involving the PIF binding pocket on the PDK1 catalytic domain and the hydrophobic motif found on the C-tail of the other kinase (34). This interaction has been shown to dramatically enhance PDK1 catalytic activity and cellular function (34). In contrast, homodimerization facilitated by interactions

between the catalytic and PH domains has been speculated to down-regulate PDK1 activity in cells (60). In the protein kinase C-related protein 2 (PRK2) an inhibitory homodimerization occurs between the N-terminal regulatory domains (including a C2 domain) and the catalytic domains (26). The AGC Rho-associated kinase I and II (ROCKI and -II) are also observed forming a homodimer between regulatory domains and the C-tail (61). Although dimerization of ROCKI does not appear to grossly stimulate or inhibit kinase activity, it does alter enzyme kinetics by lowering the K_m of ATP by 60–80-fold (61). Homodimeric truncations of ROCKI and -II and subsequently MRCKβ, have been crystallized demonstrating the involvement of the C-tail at the intermolecular interface (62–64). In PKCζ an inhibitory intramolecular interaction between the C1 domain and PIF-pocket on the catalytic domain has been previously reported (14). Together these studies suggest that domain-domain interactions in either an intermolecular or intramolecular context are common regulatory mechanisms in AGC kinases. Furthermore, they hint at the recurrence of particular domain-domain interactions such as between the C1 and AGC kinase C-tail domains. Detailed studies in related kinases are necessary to further our understanding of AGC kinase regulation. However, as we report here, the domains involved in auto-inhibitory interactions in PKCα also engage under activated conditions. The conformational flexibility apparent in multidomain interactions belies traditional structural approaches including x-ray crystallography and NMR and also complicates insight gained from truncation and site-directed mutagenesis. As such, we propose that the SPASM technique can bridge the gap between our knowledge of modular domain structure and multiplexed cellular function.

REFERENCES

1. Copley, R. R., Schultz, J., Ponting, C. P., and Bork, P. (1999) Protein families in multicellular organisms. *Curr. Opin. Struct. Biol.* **9,** 408–415
2. Lander, E. S., *et al.* (2001) Initial sequencing and analysis of the human genome. *Nature* **409,** 860–921
3. Pawson, T., and Nash, P. (2003) Assembly of cell regulatory systems through protein interaction domains. *Science* **300,** 445–452
4. Bhattacharyya, R. P., Reményi, A., Yeh, B. J., and Lim, W. A. (2006) Domains, motifs, and scaffolds: the role of modular interactions in the evolution and wiring of cell signaling circuits. *Annu. Rev. Biochem.* **75,** 655–680
5. Letunic, I., Doerks, T., and Bork, P. (2012) SMART 7: recent updates to the protein domain annotation resource. *Nucleic Acids Res.* **40,** D302–D305
6. Steinberg, S. F. (2008) Structural basis of protein kinase C isoform function. *Physiol. Rev.* **88,** 1341–1378
7. Yang, Q., and Guan, K. L. (2007) Expanding mTOR signaling. *Cell Res.* **17,** 666–681
8. Tesmer, J. J. (2009) Structure and function of regulator of G protein signaling homology domains. *Prog. Mol. Biol. Transl. Sci.* **86,** 75–113
9. Ritt, M., Guan, J. L., and Sivaramakrishnan, S. (2013) Visualizing and manipulating focal adhesion kinase regulation in live cells. *J. Biol. Chem.* **288,** 8875–8886
10. Sivaramakrishnan, S., and Spudich, J. A. (2011) Systematic control of protein interaction using a modular ER/K α-helix linker. *Proc. Natl. Acad. Sci. U.S.A.* **108,** 20467–20472
11. Slater, S. J., Seiz, J. L., Cook, A. C., Buzas, C. J., Malinowski, S. A., Kershner, J. L., Stagliano, B. A., and Stubbs, C. D. (2002) Regulation of PKCα activity by C1-C2 domain interactions. *J. Biol. Chem.* **277,** 15277–15285
12. Stensman, H., and Larsson, C. (2007) Identification of acidic amino acid residues in the protein kinase C α V5 domain that contribute to its insensitivity to diacylglycerol. *J. Biol. Chem.* **282,** 28627–28638
13. Ziemba, B. P., Li, J., Landgraf, K. E., Knight, J. D., Voth, G. A., and Falke, J. J. (2014) Single-molecule studies reveal a hidden key step in the activation mechanism of membrane-bound protein kinase Cα. *Biochemistry* **53,** 1697–1713
14. Lopez-Garcia, L. A., Schulze, J. O., Fröhner, W., Zhang, H., Süss, E., Weber, N., Navratil, J., Amon, S., Hindie, V., Zeuzem, S., Jørgensen, T. J., Alzari, P. M., Neimanis, S., Engel, M., and Biondi, R. M. (2011) Allosteric regulation of protein kinase PKCζ by the N-terminal C1 domain and small compounds to the PIF-pocket. *Chem. Biol.* **18,** 1463–1473
15. Sivaramakrishnan, S., Spink, B. J., Sim, A. Y., Doniach, S., and Spudich, J. A. (2008) Dynamic charge interactions create surprising rigidity in the ER/K α-helical protein motif. *Proc. Natl. Acad. Sci. U.S.A.* **105,** 13356–13361
16. Sivaramakrishnan, S., Sung, J., Ali, M., Doniach, S., Flyvbjerg, H., and Spudich, J. A. (2009) Combining single-molecule optical trapping and small-angle x-ray scattering measurements to compute the persistence length of a protein ER/K α-helix. *Biophys. J.* **97,** 2993–2999
17. Malik, R. U., Ritt, M., DeVree, B. T., Neubig, R. R., Sunahara, R. K., and Sivaramakrishnan, S. (2013) Detection of G protein-selective G protein-coupled receptor (GPCR) conformations in live cells. *J. Biol. Chem.* **288,** 17167–17178
18. Leonard, T. A., Ró¿zycki, B., Saidi, L. F., Hummer, G., and Hurley, J. H. (2011) Crystal structure and allosteric activation of protein kinase C βII. *Cell* **144,** 55–66
19. Violin, J. D., Zhang, J., Tsien, R. Y., and Newton, A. C. (2003) A genetically encoded fluorescent reporter reveals oscillatory phosphorylation by protein kinase C. *J. Cell Biol.* **161,** 899–909
20. Huang, S. M., Leventhal, P. S., Wiepz, G. J., and Bertics, P. J. (1999) Calcium and phosphatidylserine stimulate the self-association of conventional protein kinase C isoforms. *Biochemistry* **38,** 12020–12027
21. Giorgione, J., and Newton, A. C. (2003) Measuring the binding of protein kinase C to sucrose-loaded vesicles. *Methods Mol. Biol.* **233,** 105–113
22. Kirwan, A. F., Bibby, A. C., Mvilongo, T., Riedel, H., Burke, T., Millis, S. Z., and Parissenti, A. M. (2003) Inhibition of protein kinase C catalytic activity by additional regions within the human protein kinase Cα-regulatory domain lying outside of the pseudosubstrate sequence. *Biochem. J.* **373,** 571–581
23. Braun, D. C., Garfield, S. H., and Blumberg, P. M. (2005) Analysis by fluorescence resonance energy transfer of the interaction between ligands and protein kinase Cδ in the intact cell. *J. Biol. Chem.* **280,** 8164–8171
24. van Duuren, B. L., Banerjee, S., and Witz, G. (1976) Fluorescence studies on the interaction of the tumor promoter phorbol myristate acetate and related compounds with rat liver plasma membranes. *Chem. Biol. Interact.* **15,** 233–246
25. Yang, L., and Glaser, M. (1996) Formation of membrane domains during the activation of protein kinase C. *Biochemistry* **35,** 13966–13974
26. Bauer, A. F., Sonzogni, S., Meyer, L., Zeuzem, S., Piiper, A., Biondi, R. M., and Neimanis, S. (2012) Regulation of protein kinase C-related protein kinase 2 (PRK2) by an intermolecular PRK2-PRK2 interaction mediated by Its N-terminal domain. *J. Biol. Chem.* **287,** 20590–20602
27. Mochly-Rosen, D., and Koshland, D. E., Jr. (1987) Domain structure and phosphorylation of protein kinase C. *J. Biol. Chem.* **262,** 2291–2297
28. Walker, J. M., and Sando, J. J. (1988) Activation of protein kinase C by short chain phosphatidylcholines. *J. Biol. Chem.* **263,** 4537–4540
29. Flint, A. J., Paladini, R. D., and Koshland, D. E., Jr. (1990) Autophosphorylation of protein kinase C at three separated regions of its primary sequence. *Science* **249,** 408–411
30. Nishizuka, Y. (1988) The molecular heterogeneity of protein kinase C and its implications for cellular regulation. *Nature* **334,** 661–665
31. Yeong, S. S., Zhu, Y., Smith, D., Verma, C., Lim, W. G., Tan, B. J., Li, Q. T., Cheung, N. S., Cai, M., Zhu, Y. Z., Zhou, S. F., Tan, S. L., and Duan, W. (2006) The last 10 amino acid residues beyond the hydrophobic motif are critical for the catalytic competence and function of protein kinase Cα. *J. Biol. Chem.* **281,** 30768–30781
32. Ni, Q., Shaffer, J., and Adams, J. A. (2000) Insights into nucleotide binding in protein kinase A using fluorescent adenosine derivatives. *Protein Sci.* **9,** 1818–1827
33. Keshwani, M. M., and Harris, T. K. (2008) Kinetic mechanism of fully

activated S6K1 protein kinase. *J. Biol. Chem.* **283,** 11972–11980
34. Biondi, R. M., Cheung, P. C., Casamayor, A., Deak, M., Currie, R. A., and Alessi, D. R. (2000) Identification of a pocket in the PDK1 kinase domain that interacts with PIF and the C-terminal residues of PKA. *EMBO J.* **19,** 979–988
35. Sando, J. J., Chertihin, O. I., Owens, J. M., and Kretsinger, R. H. (1998) Contributions to maxima in protein kinase C activation. *J. Biol. Chem.* **273,** 34022–34027
36. Raghunath, A., Ling, M., and Larsson, C. (2003) The catalytic domain limits the translocation of protein kinase C α in response to increases in Ca^{2+} and diacylglycerol. *Biochem. J.* **370,** 901–912
37. Schmalz, D., Hucho, F., and Buchner, K. (1998) Nuclear import of protein kinase C occurs by a mechanism distinct from the mechanism used by proteins with a classical nuclear localization signal. *J. Cell Sci.* **111,** 1823–1830
38. Castagna, M., Takai, Y., Kaibuchi, K., Sano, K., Kikkawa, U., and Nishizuka, Y. (1982) Direct activation of calcium-activated, phospholipid-dependent protein kinase by tumor-promoting phorbol esters. *J. Biol. Chem.* **257,** 7847–7851
39. van Corven, E. J., Groenink, A., Jalink, K., Eichholtz, T., and Moolenaar, W. H. (1989) Lysophosphatidate-induced cell proliferation: identification and dissection of signaling pathways mediated by G proteins. *Cell* **59,** 45–54
40. Dubin, A. E., Herr, D. R., and Chun, J. (2010) Diversity of lysophosphatidic acid receptor-mediated intracellular calcium signaling in early cortical neurogenesis. *J. Neurosci.* **30,** 7300–7309
41. Pearce, L. R., Komander, D., and Alessi, D. R. (2010) The nuts and bolts of AGC protein kinases. *Nat. Rev. Mol. Cell Biol.* **11,** 9–22
42. House, C., and Kemp, B. E. (1987) Protein kinase C contains a pseudosubstrate prototope in its regulatory domain. *Science* **238,** 1726–1728
43. Kannan, N., Haste, N., Taylor, S. S., and Neuwald, A. F. (2007) The hallmark of AGC kinase functional divergence is its C-terminal tail, a cis-acting regulatory module. *Proc. Natl. Acad. Sci. U.S.A.* **104,** 1272–1277
44. Guo, B., Reed, K., and Parissenti, A. M. (2006) Scanning mutagenesis studies reveal multiple distinct regions within the human protein kinase C α regulatory domain important for phorbol ester-dependent activation of the enzyme. *J. Mol. Biol.* **357,** 820–832
45. Bornancin, F., and Parker, P. J. (1997) Phosphorylation of protein kinase Cα on serine 657 controls the accumulation of active enzyme and contributes to its phosphatase-resistant state. *J. Biol. Chem.* **272,** 3544–3549
46. Stensman, H., Raghunath, A., and Larsson, C. (2004) Autophosphorylation suppresses whereas kinase inhibition augments the translocation of protein kinase Cα in response to diacylglycerol. *J. Biol. Chem.* **279,** 40576–40583
47. Hauge, C., Antal, T. L., Hirschberg, D., Doehn, U., Thorup, K., Idrissova, L., Hansen, K., Jensen, O. N., Jørgensen, T. J., Biondi, R. M., and Frödin, M. (2007) Mechanism for activation of the growth factor-activated AGC kinases by turn motif phosphorylation. *EMBO J.* **26,** 2251–2261
48. Grodsky, N., Li, Y., Bouzida, D., Love, R., Jensen, J., Nodes, B., Nonomiya, J., and Grant, S. (2006) Structure of the catalytic domain of human protein kinase C βII complexed with a bisindolylmaleimide inhibitor. *Biochemistry* **45,** 13970–13981
49. Dutil, E. M., and Newton, A. C. (2000) Dual role of pseudosubstrate in the coordinated regulation of protein kinase C by phosphorylation and diacylglycerol. *J. Biol. Chem.* **275,** 10697–10701
50. Roberts, P. J., and Der, C. J. (2007) Targeting the Raf-MEK-ERK mitogen-activated protein kinase cascade for the treatment of cancer. *Oncogene* **26,** 3291–3310
51. Cameron, A. J., Escribano, C., Saurin, A. T., Kostelecky, B., and Parker, P. J. (2009) PKC maturation is promoted by nucleotide pocket occupation independently of intrinsic kinase activity. *Nat. Struct. Mol. Biol.* **16,** 624–630
52. Liu, Q., and Molkentin, J. D. (2011) Protein kinase Cα as a heart failure therapeutic target. *J. Mol. Cell. Cardiol* **51,** 474–478
53. Alkon, D. L., Sun, M. K., and Nelson, T. J. (2007) PKC signaling deficits: a mechanistic hypothesis for the origins of Alzheimer's disease. *Trends Pharmacol. Sci.* **28,** 51–60
54. Geraldes, P., and King, G. L. (2010) Activation of protein kinase C isoforms and its impact on diabetic complications. *Circ. Res.* **106,** 1319–1331
55. Tam, W. L., Lu, H., Buikhuisen, J., Soh, B. S., Lim, E., Reinhardt, F., Wu, Z. J., Krall, J. A., Bierie, B., Guo, W., Chen, X., Liu, X. S., Brown, M., Lim, B., and Weinberg, R. A. (2013) Protein kinase Cα is a central signaling node and therapeutic target for breast cancer stem cells. *Cancer Cell* **24,** 347–364
56. Kheifets, V., and Mochly-Rosen, D. (2007) Insight into intra- and intermolecular interactions of PKC: design of specific modulators of kinase function. *Pharmacol. Res.* **55,** 467–476
57. Oancea, E., and Meyer, T. (1998) Protein kinase C as a molecular machine for decoding calcium and diacylglycerol signals. *Cell* **95,** 307–318
58. Rosse, C., Linch, M., Kermorgant, S., Cameron, A. J., Boeckeler, K., and Parker, P. J. (2010) PKC and the control of localized signal dynamics. *Nat. Rev. Mol. Cell Biol.* **11,** 103–112
59. Huang, K. P. (1989) The mechanism of protein kinase C activation. *Trends Neurosci.* **12,** 425–432
60. Masters, T. A., Calleja, V., Armoogum, D. A., Marsh, R. J., Applebee, C. J., Laguerre, M., Bain, A. J., and Larijani, B. (2010) Regulation of 3-phosphoinositide-dependent protein kinase 1 activity by homodimerization in live cells. *Sci. Signal.* **3,** ra78
61. Doran, J. D., Liu, X., Taslimi, P., Saadat, A., and Fox, T. (2004) New insights into the structure-function relationships of Rho-associated kinase: a thermodynamic and hydrodynamic study of the dimer-to-monomer transition and its kinetic implications. *Biochem. J.* **384,** 255–262
62. Jacobs, M., Hayakawa, K., Swenson, L., Bellon, S., Fleming, M., Taslimi, P., and Doran, J. (2006) The structure of dimeric ROCK I reveals the mechanism for ligand selectivity. *J. Biol. Chem.* **281,** 260–268
63. Heikkila, T., Wheatley, E., Crighton, D., Schroder, E., Boakes, A., Kaye, S. J., Mezna, M., Pang, L., Rushbrooke, M., Turnbull, A., and Olson, M. F. (2011) Co-crystal structures of inhibitors with MRCKβ, a key regulator of tumor cell invasion. *PLoS ONE* **6,** e24825
64. Yamaguchi, H., Kasa, M., Amano, M., Kaibuchi, K., and Hakoshima, T. (2006) Molecular mechanism for the regulation of rho-kinase by dimerization and its inhibition by fasudil. *Structure* **14,** 589–600

Conserved Modular Domains Team up to Latch-open Active Protein Kinase Cα

Carter J. Swanson, Michael Ritt, William Wang, Michael J. Lang, Arvind Narayan, John J. Tesmer, Margaret Westfall and Sivaraj Sivaramakrishnan

J. Biol. Chem. 2014, 289:17812-17829.
doi: 10.1074/jbc.M113.534750 originally published online April 30, 2014
